IEEE Access
Multidisciplinary | Rapid Review | Open Access Journal

Received February 11, 2020, accepted February 23, 2020, date of publication February 27, 2020, date of current version March 11, 2020.

Digital Object Identifier 10.1109/ACCESS.2020.2976828

A Novel Hybrid Ant Colony-Particle Swarm Optimization Techniques Based Tuning STATCOM for Grid Code Compliance

OMAR MAKRAM KAMEL[1], AHMED A. ZAKI DIAB[2], TON DUC DO[3], (Senior Member, IEEE), AND MAHMOUD A. MOSSA[2]

[1]Electrical and Computer Department, El-Minia H.I.E.T., Minia 61125, Egypt
[2]Electrical Engineering Department, Faculty of Engineering, Minia University, Minia 61111, Egypt
[3]Department of Robotics and Mechatronics, School of Engineering and Digital Sciences (SEDS), Nazarbayev University, Nur-Sultan Z05H0P9, Kazakhstan

Corresponding authors: Ton Duc Do (doduc.ton@nu.edu.kz) and Mahmoud A. Mossa (mahmoud_a_mossa@mu.edu.eg)

This work was supported by the Nazarbayev University via the ORAU grant "Fault-Tolerant Direct-Torque Control System Design with High-Order Observers for Interior Permanent Magnet Synchronous Motors in Electric Vehicle Applications", Grant No. SST2017030.

ABSTRACT Integrating wind power plants (WPPs) into power systems are increasing dramatically now a day. However, the dynamic performance of power systems will be affected by the large penetration level of such renewable sources of energy. From this context power system operators and transmission system operators have put regulation rules to keep pushing wind power plants to safeguard limits that keep power system more stable and reliable. One of these rules is providing a low voltage ride through (LVRT) for wind farms without disconnecting it from the power system. The current paper implements the STATCOM as a LVRT for a 9 MW wind farm connected to the grid through transmission system of 120 kV. For enhancing the dynamic performance of STATCOM, two types of optimization methodologies: ant colony (ACO) and particle swarm optimization (PSO), are proposed to fine tune the coefficients of PI controllers to optimally manage the STATCOM dynamics.

INDEX TERMS Fuzzy controller, PI, STATCOM, PSO, ACO, HPA, DFIG, WT, VSC, THD.

I. INTRODUCTION

Concerns about climate changes are increasing nowadays, causing many countries moving their attitudes towards renewable energy sources. According to the international renewable energy agency (IRENA), the integration of renewable energy into the power systems is hurriedly growing [1]. The energy markets have been occupied by different types of electric energy suppliers, within which the wind power (WP) was the most influencing and most developing sources [2].

Variable speed doubly fed induction generator (DFIG) has been extensively utilized for converting the wind power into electrical energy; this is due to the capability of the DFIG to provide a fixed voltage and fixed frequency even with a variable input wind speed. Moreover, such systems have the advantages of low cost of back-to-back converters [3], [4]. On the other hand, due to the limited capability of DFIG in regulating the reactive power under severe fault conditions, additional equipment such as STATCOM is added to the WT-DFIG for tracking grid code requirements and getting adequate low voltage ride through (LVRT). The grid codes argue with the necessity of keeping the WPs integration into the utility grid under severe fault conditions to enhance the reliability and stability. Under grid voltage sags, the operation of wind driven DFIG is interrupted and as a result, it concludes by disconnecting the generation unit from the grid [5], [7]. Disconnecting the wind driven DFIG from the grid is not an acceptable action, mainly when WP contributes with a remarkable portion of the total grid power. The LVRT is the most commonly adopted ride-through technique which is used when a voltage sage condition is present; it has the ability to maintain the controllability of the system under such operations [9], [10]. Besides providing LVRT capability, WP must have the ability to assist the reactive power during faults period to ensure fast recovering of active power after clearing the fault [6].

The associate editor coordinating the review of this manuscript and approving it for publication was Zhouyang Ren.

Several control approaches have been proposed to achieve a co-ordinated control between the grid side converter (GSC) and rotor side converter (RSC) of the DFIG under non-severe voltage sags conditions, but few studies which have investigated the deep voltage sags. The problems of deep voltage sags arise from the failure in keeping the rotor current control due to the over-modulation occurred at the RSC as a result to the large electromotive force (EMF) subjected to the rotor terminals.

As a solution for this issue, the researchers in [8] have proposed an effective voltage control technique to regulate the operations of GSC and RSC during different types of system faults. In [11], an improved field oriented control (FOC) has been utilized to improve the dynamic response under different fault conditions and the LVRT capability is realized. In previous studies, the GSC has been used as a STATCOM to provide the DFIG with the magnetization demands; even though, under weak grid and for severe voltage sags, the GSC fails in providing the required magnetizing power and assists the voltage balance due to the reduced power rate (about 30 % of rated power, which increases the voltage instability. Despite of the restricted power rating of the rotor converter, the converter still has the ability to support the system instability by keeping generating of reactive power eventhough this happens within a limited rate and under mild fault conditions, as reported in [39], [40]. In addition to, variable speed has been obtained operation between 0.7 pu and 1.2 pu [41]. According to the analysis performed in, the industrial design of these converters provides additional operating limitation that can reach up to 50% of the rated power, which suggest means additional operating margins. Therefore, choosing proper control technique can support DFIGs with reactive power to improve the post-fault voltage profile by damping oscillation and preventing over-shoots. However, under large disturbances and due to the reactive power capability limits of the DFIG, the control circuits of both rotor side and grid side converters became over-modulated and hence lose their ability to provide the DFIG with the necessary magnetizing power. Under such circumstances, FACTS devices especially STATCOMs become a vital element that can support WPP dynamic performance and keep it tracking the associated grid code requirements [42].

It is worth to mention that, the requirement for an external reactive power regulator is not only a requirement for the DFIG as a generating unit, but also for other types of generators such as permanent magnet synchronous generator (PMSG). Even though, the PMSG is connected directly to the grid via a grid-side converter (GSC) which has a higher power rating compared to that of the rotor side converter of the DFIG; but for a deep voltage drop in the grid (due to severe faults), the power transferring from the DC-link of the converter to the grid will decrease drastically due to the limitations of the converter's current [43]. On the other side, the generating of the power is still present, which finally results in a rapid increase of DC link voltage. Moreover, under asymmetrical grid fault conditions, the negative sequence components of stator voltage and current result in increasing the total harmonic distortion (THD).

As a quick action, the utilities isolate the wind turbine from the universal grid to avoid a risk condition. Under these situations, maintaining the voltage stability will be the most critical argument for preserving a continuous and stable duty for the wind driven DFIG. This issue can be handled via utilizing external units such as STATCOM. The implementation of the STATCOM is for imposing the reactive power to the system at the PCC and dynamic voltage restore (DVR) as well [6], [12]. STATCOM has been extensively adopted to enhance the system dynamics under severe grid conditions at the point of connection (PCC) with the wind driven DFIG [26]. However, investigating the effectiveness of STATCOM in improving the electric dynamics of the utility grid under fault conditions is still requiring more studies. In study [27], the artificial neural network is implemented to adapt and tune the parameters of STATCOM's PI controller to regulate the reactive power feeding process for power system; this method saves effectively the time but still requires high number of iterations for testing and training each neural. In [28], an efficient voltage controller is adopted to enhance the performance of STATCOM in order to realize LVRT ability for a wind turbine rotating with a fixed speed.

In an attempt to mitigate and limit the negative effects of voltage sages under severe fault conditions, in the current study presented by this paper the dynamic performance of STATCOM is analyzed via utilizing different biological Metaheuristic techniques, while the main target is keeping the wind driven DFIG still following the standard grid codes. Evolutionary algorithms (EAs) are considered as stochastic search mechanisms. These algorithms emulate the dynamic of biological evolution or the species social behavior. The species follows or tracks the other members by evolution, adaptation and learning [18]. These Meta-heuristic algorithms are considered as elementary approaches which can achieve competent, but not essentially optimum solutions to high sophisticated problems [13].

Motivated by the previous review, in this paper there are four methods have been considered for adapting the coefficients of PI regulators to manipulate the dynamics of STATCOM, the aforementioned algorithms are the traditional tuning (trial and error), PSO, ACO and hybrid PSO-ACO. A complete comparison is performed to prove that these new biological methods can be adapted to solve complicated problems with a very promising result while saving time and effort by providing an acceptable LVR for the wind farm and keeping it compliance with the grid codes.

II. SYSTEM LAYOUT

Figure 1 illustrates a six 1.5 MW wind turbine-DFIGs constituting a 9 MW wind farm. In this system three phase transformers with rating of 575V/25 kV connects the wind

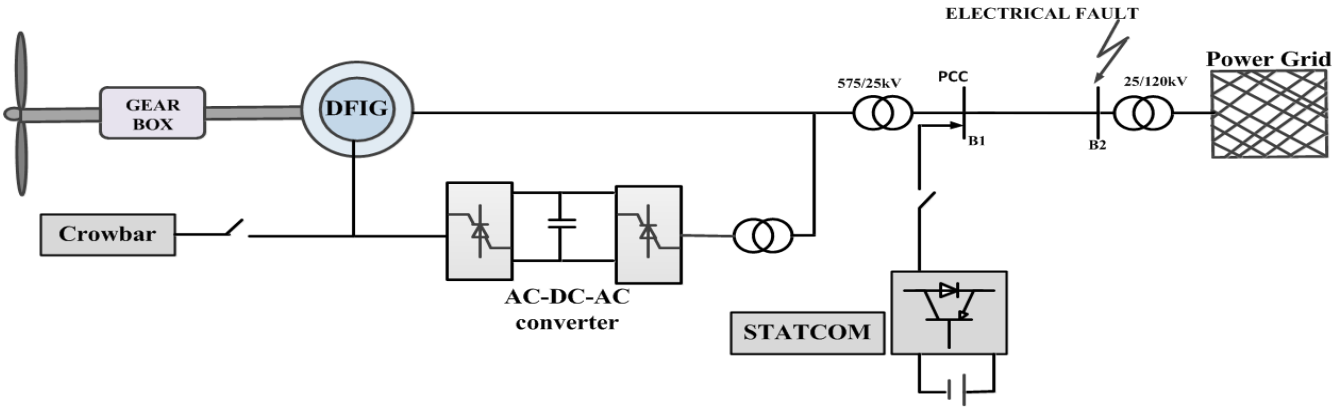

FIGURE 1. Overall layout for the system under study.

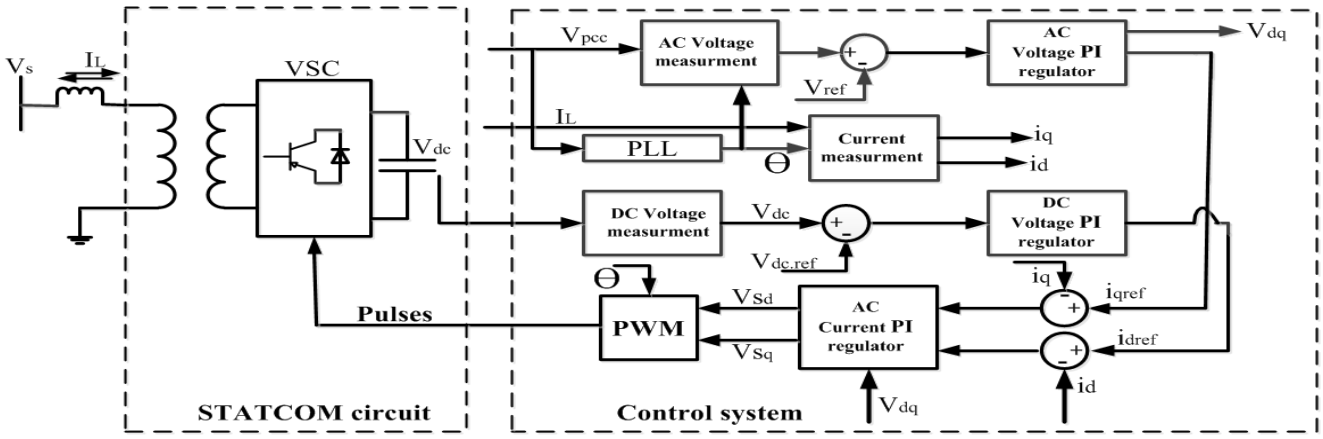

FIGURE 2. Configuration of STATCOM and its control circuit.

farm to a 25 kV distribution system at B1. A medium line of 30 Km length transfers the power from the wind turbine-DFIG system to the 120 kV power grid using three phase transformer of 25/120 kV at feeder B2. For the DFIGs, the rotor terminals are connected to the grid through an AC/DC/AC IGBT-based PWM converter, while stator terminals are connected to the grid via a step-up transformer. The bus bars B1 and B2 are referring to the sending and the receiving endpoints, respectively. Near B2 it is claimed that there are severe fault conditions and the system dynamics and power system stability are analyzed.

III. STATCOM MODELING

Flexible AC transmission lines (FACTS) are very important elements found in the modern AC power systems that based on the renewable energy [15]. STATCOM that belongs to the FACTS devices can improve the dynamic performance of wind power plants during the un-predicted situations, hence makes the integration of such renewable energy sources into the power grids more reliable. STATCOM is voltage a source converter but its behavior is not the same as the static voltage converter (SVC), because it can provide a full operating range by absorbing or generating reactive power according to system situation [14]. The point at which the STATCOM is connected is considered as the voltage control point, where the active and reactive power flow can be regulated and controlled through the STATCOM operating condition. The basic construction of the STATCOM is based on two voltage source converter (VSC) with an intermediated DC-link capacitor, and a shunt transformer connects the STATCOM terminals to the AC transmission lines.

A. STATCOM BASIC CONSTRUCTION

Figure 2 shows the basic construction and the control circuit of the STATCOM. Synchronization between the SATCOM voltage and utility voltage is performed by the phase locked loop (PLL), where the $\ominus$ value of the PLL computes the d-q components of voltages and currents. Both the AC voltage and the DC-link controllers represent the outer regulation loop, where the I_q current component is responsible for regulating the reactive power, the I_d current component pertained to regulate the active power. The phase angle and magnitude of the voltage generated by the PWM converter can be controlled through the current regulators according to the values

of I_{qref}, I_{dref} which are obtained from the DC-link voltage and AC voltage regulators, respectively.

The active and reactive powers may be expressed as by the following equations,

$$P = \frac{V_{PCC} * V_S}{X} sin\ \delta \tag{1}$$

$$Q = \frac{V_{PCC}(V_{PCC} - V_S cos\ \delta)}{X} \tag{2}$$

where V_{PCC} is the PCC system voltage, V_S is the STATCOM voltage, δ is the angle of V_g with respect to V_S (this angle is set to zero for reactive power control only), and X is the reactance value for line connection between V_{PCC} and V_S.

Thus, to regulate the reactive power current component, an internal feedback loop is utilized. This action can be also realized through adapting the angle difference between the system voltage ($\boldsymbol{V_{PCC}}$) and the reactive power current component.

B. STATCOM CONTROL TOPOLOGY

The STATCOM control circuit is illustrated in Figure 2. In this circuit, the PLL is utilized for synchronizing the system's three phase voltage ($V1$), the PLL angle $\ominus$ is then used to calculate the direct and quadrature axis components of the voltages and currents. The DC and AC regulators constitute the outer adaptation loop in the controller.

The task of the I_{dref} and I_{qref} current regulators is to control the amplitude and phase angle of the voltages obtained from the PWM converter. So, the reactive power current component is regulated through an inner feedback loop an inner feedback loop. The operation of the current regulator is based upon adjusting the phase difference between the system voltage and the developed reactive power current component. For simplicity and for saving the computational time, the equivalent circuit model of the STATCOM is used instead of the MMC-STATCOM, this is to save the time taken to evaluate the parameters of STATCOM using the optimization techniques (online-adaptation). However the DC-link response of the STATCOM was taken into account during evaluating the parameters for faster and better performance of STATCOM.

It is clear that the MMC-STATCOM gives better performance for reactive power compensation, harmonic rejection, and for balancing system performance under disturbances. However, it needs more control circuits which mean larger time consumption [42].

IV. ADAPTATION MECHANISM OF PI PARAMETERS

For regulating the STATCOM operating conditions, the PI regulators are extensively adopted as a vital solution to acquire an acceptable behavior [21], [22] and [24]. The disadvantage of traditional parameters tuning methods is that its dynamic performance becomes unstable when the system changes its operating state, and to avoid this shortage, the non-linear regulator is utilized to enhance the control capability in evaluating the most accurate parameters according to the system operating conditions.

For conventional tuning of PI parameters used for both experimental and simulated systems, an expert system (ES) based upon trial and error method is usually adopted. In the past several commercial auto-tuned PI controllers for general purpose, higher order linear control system was available. The expert controller contains the knowledge base of tuning the controller.

PI controllers are most commonly adopted for controlling the STATCOM operation to realize a better dynamic performance thanks to its simplicity, robustness, and wide applicability. There are several tuning algorithms which have been presented for the internal gains of PI controllers, to obtain better and more definite response for the control process. The traditional methods used for tuning the parameters of PI regulators are Ziegler- Nicholas method, Tyreus-Luyben method, and Damped oscillation method. The most commonly used method is the Ziegler- Nicholas technique which provides better response besides minimizing the absolute error. The dynamics of this method can be described as follows,

$$G(S) = K_p + \frac{1}{K_i S} \tag{3}$$

where, K_p and K_i are the proportional and integral constants according to Ziegler- Nicholas,

$$K_p = 0.45K_{cu} \quad \text{and} \quad K_i = \frac{P_u}{1.2} \tag{4}$$

where K_{cu} and P_u are the ultimate gain and frequency.

Based on the control circuit of STATCOM illustrated in Figure 4, the STATCOM's reactive power is given by,

$$Q_{ST} = V_{ST} I_{ST} \tag{5}$$

$$I_{ST} = K_p \left(V_{ref} - V_{pcc}\right) / T_r \tag{6}$$

where I_{ST} and Q_{ST} are the STATCOM current and reactive power respectively, V_{ST} is the STATCOM voltage, and K_p, T_r are the proportional gains and time constant of the STATCOM controller.

For a 1/4 decay ratio the transfer function of PI controller is as

$$G(S) = 0.75K_{cu}P_u \left(\frac{S + \frac{4}{P_u}}{S}\right) \tag{7}$$

Thus the PI controller has a pole at the origin and double zeros at $S = -4/P_u$.

On the other hand, this method is suffering from some deficiencies such as consuming large time as it is based on the trial and error procedure; this is besides the performance degradation under the up normal system operating condition. Thus, new techniques such as internal model control, artificial intelligence and FUZZY logic methods are adopted to overcome these shortages. Recently optimization methods are harnessed for adapting the PI controller gains as introduced here in the following subsections.

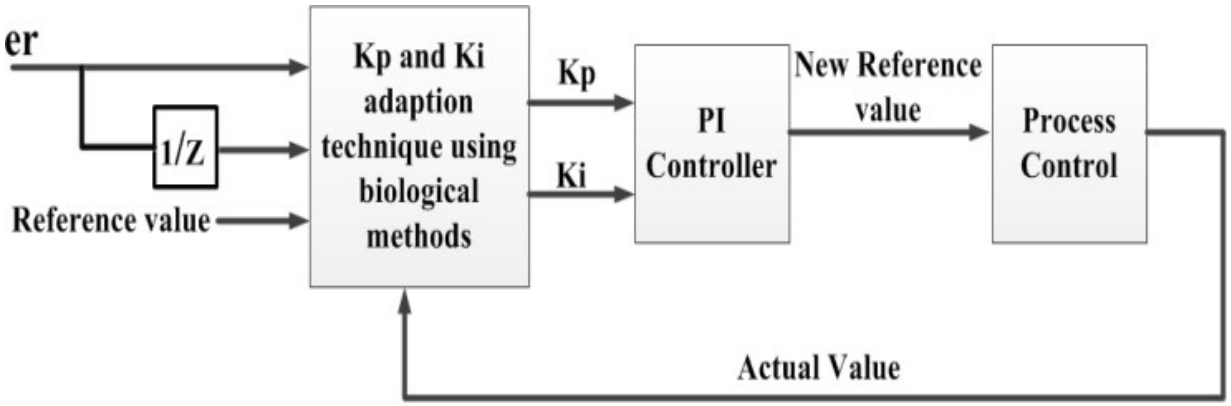

FIGURE 3. PI parameter adaptation using biological methods.

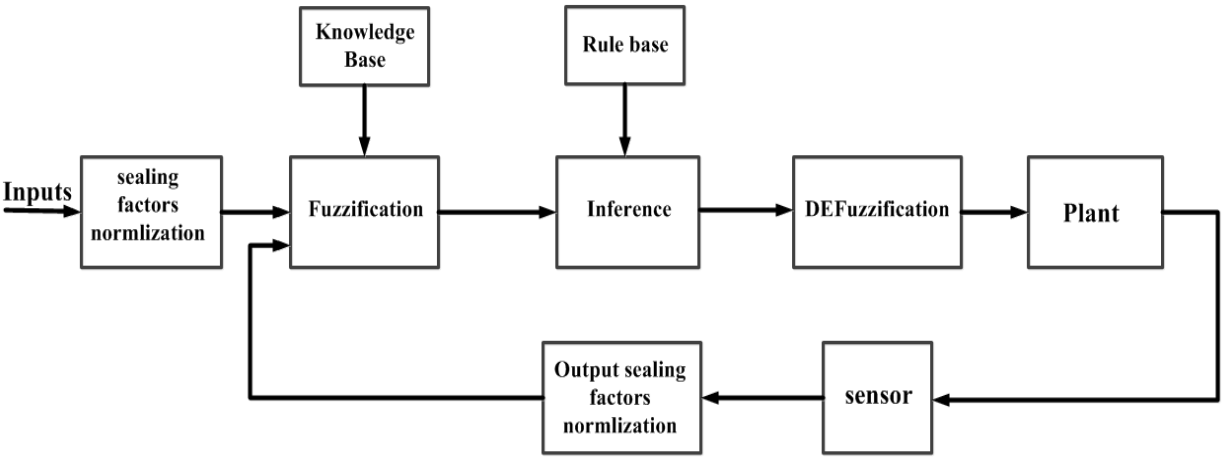

FIGURE 4. Layout of FUZZY controller.

Recently, via adopting either evolutionary methods such as PSO and ACO or artificial methods such as fuzzy, an improvement in the PI dynamic performance can be achieved via determining and using the most appropriate values for K_i and K_p coefficients based on system situation statues. The following section describes how PSO, ACO and FUZZY are used for tuning PI parameters to realize improved dynamic performance for STATCOM. Figure 3 shows the adaptation process of the proposed non-linear techniques used for tuning the PI parameters.

A. FUZZY CONTROLLER

FUZZY control does not strictly need any mathematical model of the plant. It is based on plant operator experience and heuristics, and it is very easy to apply [25]. Fuzzy control is basically an adaptive and non-linear control, which gives a robust performance for non-linear plant with parameter variation [26], [27]. The block diagram for FUZZY controller is shown in Figure 4. The Knowledge base module contains knowledge and data about all the input and output of FUZZY partitions also it includes the term set and the corresponding membership functions defining the input variables to the FUZZY rule base system and the output variables or control actions to the plant under control.

Since the FUZZY controller is basically an input/output static nonlinear mapping, it can be used to formalize the following control action for the PI controller [27], [28],

$$K_1E + K_2E = DU \tag{8}$$

where K_1 and K_2 are non-linear coefficients obtained from FUZZY controller. E is the error representing FUZZY input. The controller output is the DU which is integrated to obtain the new reference signal as following,

$$U = \int DU\,dt = K_1 \int E\,dt + K_2 \int cE\,dt \tag{9}$$

Or

$$U = K_1 \int E\,dt + K_2E \tag{10}$$

The Figure 5 illustrates adapting FUZZY logic for tuning the STATCOM's PI controllers.

The nonlinear adaptive gains FUZZY controller, which are varied on-line give the power to the FUZZY logic controller

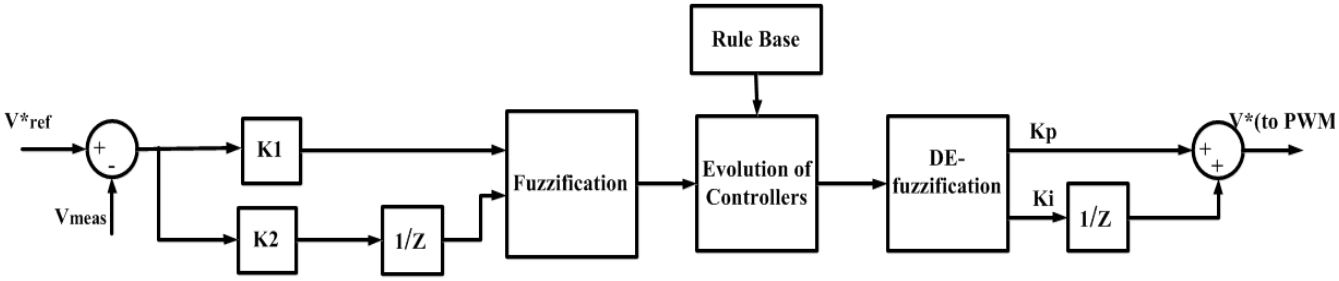

FIGURE 5. FUZZY controller as a PI regulator.

to make the system response robust in the presence of different disturbance conditions. The input scaling factors $\boldsymbol{K_1}$ and $\boldsymbol{K_2}$ can be constant or programmable which can control the sensitivity of the operation.

B. TUNING OF PI CONTROLLER USING PARTICLE SWARM OPTIMIZATION (PSO)

PSO is an optimization technique which was designed in 1995 by Eberhart and Kenedy based on the birds' flocking social attitudes [18]. The PSO has two main stages to be implemented, the exploration and exploitation [29], [30].

The operation principle of PSO can be described as follows:

Firstly the locations of local particles in the search area are updated according to the following expression,

$$X_{k+1}^{i} = X_{k}^{i} + V_{k+1}^{i} \tag{11}$$

where the velocity of the particles V_{k+1}^{i} is calculated by

$$V_{k+1}^{i} = V_{k}^{i} + C_1 r_1 \left(P_{k}^{i} - X_{k}^{i}\right) + C_2 r_2 \left(P_{k}^{g} - X_{k}^{i}\right) \tag{12}$$

where X_k^i is the particle location, V_k^i is the particle velocity, P_k^i is the optimal position of the specified particle, P_k^g is the optimal location of the swarm, C_1 and C_2 are the cognitive and social parameters and r_1 and r_2 are numbers selected randomly between 0 and 1.

The sequence of implementing the PSO algorithm can be verified by the following steps

1-**Intialize**

a- set constants C_1 and C_2 number of particles (K).
b- initialize particle positions randomly.
c- initialize particle velocities randomly.
d- set iter = 1.

2-**Optimize**

a - evaluate the function value F_k^i using design space coordinates X_k^i.
b - if $F_k^i \le F_{best}^i$ then $F_{best}^i = F_k^i, P_k^i = X_k^i$.
c - if $F_k^i \le F_g^i$ then $F_{best}^g = F_k^i, P_k^g = X_k^i$.
d - if stopping condition is satisfied, then go to step 3.
E - update all particle velocities if V_k^i for i = 1..... P.
f - update all particle positions if X_k^i for i = 1..... P.
g - increment K.
h - Go to 2(a).

3-Terminate.

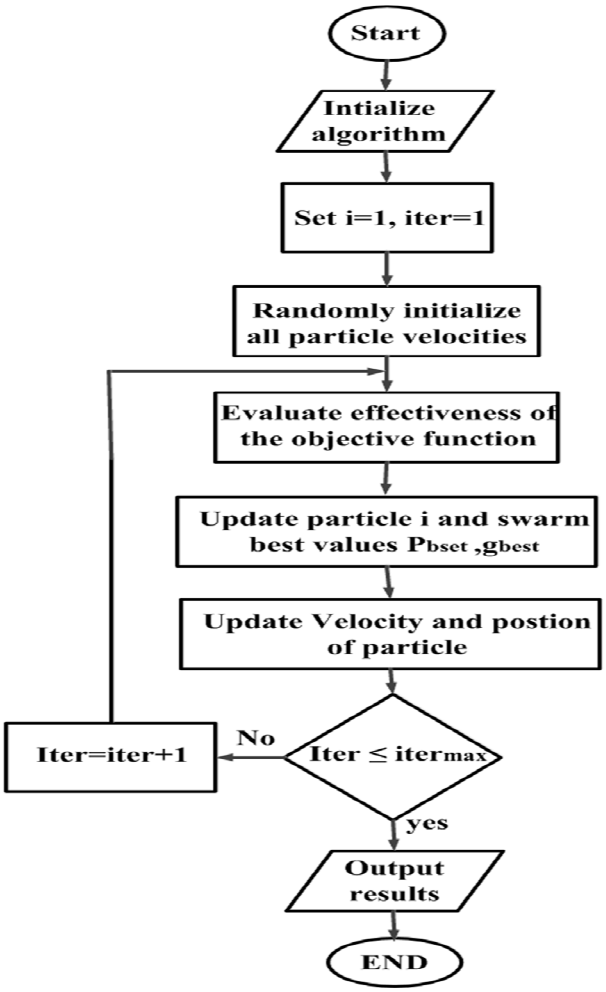

FIGURE 6. Implementation procedure for PSO-PI controller.

In the current paper, the PSO is modified to achieve precise tuning for the parameters of PI controllers used by the STATCOM so that the wind driven DFIG keeps track of grid code protocols for various types of grid faults [27], [31]–[33]. The PSO technique starts with random initialization for the values K_i and K_p then the effectiveness degree of the cost function is evaluated and weighted with respect to the desired value, afterwards the velocities and positions of the particles are updated following the prescribed rules as described earlier. The execution cycle continues until either the cost function

develops its reference value or the number of iterations reaches to its limit. The flowchart shown in Figure 6 explains the steps for PSO-PI controllers.

C. ANT COLONY AS A PI REGULATOR

The operation of ant colony optimization technique is depending on a chemical treatment (pheromone) which is provided by ants during searching for foods on the ground; this pheromone can guide effectively the other ants to walk forward the target [34]. The more ants pass through a certain path, the more pheromones are left, and this leads to increasing the probability of selecting this path by other ants. In addition, when the number of left pheromone is high, the ants can find the appropriate path to the food in shorter time. So this means that the chemical reaction developed by ants depends entirely on the number of ants which are using this path [35].

The updating mechanism for the Pheromone can be described as follows;

The pheromone of each individual ant is being left on the edges of the traveling route until the ants complete all iterations. The total number of pheromone per each edge is expressed by,

$$\tau_{ij}(t+1) = \Delta\tau_{ij} + (1-\rho)\,\tau_{ij}(t) \tag{13}$$

where τ is the pheromone mark, and ρ is the rate by which the pheromone evaporates. $\rho \in [0, 1]$.

Based on probability, the ants start to move from one place to another. At first, the accessed positions must be allocated in taboo table. After that, the available degree is defined and calculated by $\eta_{ij} = \frac{1}{d_{ij}}$. The probability by which the K^{th} ant can select between positions is defined by

$$P_{ij}(t) = \left\{ \begin{array}{cc} \frac{(\tau_{ij})^{\alpha}(\eta_{ij})^{\beta}}{\Sigma(\tau_{ik})^{\alpha}(\eta_{ik})^{\beta}} & j \in allowed\ K \\ 0.0 & else \end{array} \right\} \tag{14}$$

where α and β denote to the pheromones balancing weights. These two values are utilized to evaluate the relative impact of the route pheromone and heuristic data.

The following steps explain the initialization of the attractiveness base (τ), and visibility (η) for each ant.

For $i <$ max iteration do:
For each ant does
Choose probabilistically (based on previous equation of probability) the subsequent state to move into;
Repeat until each ant completed a solution;
End
.....For each ant that completed a solution do:
Update attractiveness (pheromone trail τ) for each ant path that traversed;
End
If (local best solution better than global solution)
Save local best solution as global solution;
End

Via analyzing the ACO operation, it can be concluded that the ACO can be utilized as a feasible tool for analyzing the graphically expressed problems. The ACO was primarily reformed to tune PI gains by [36]. The graphic illustration of ACO technique used to tune the PI parameters is shown in Figure 7.a.

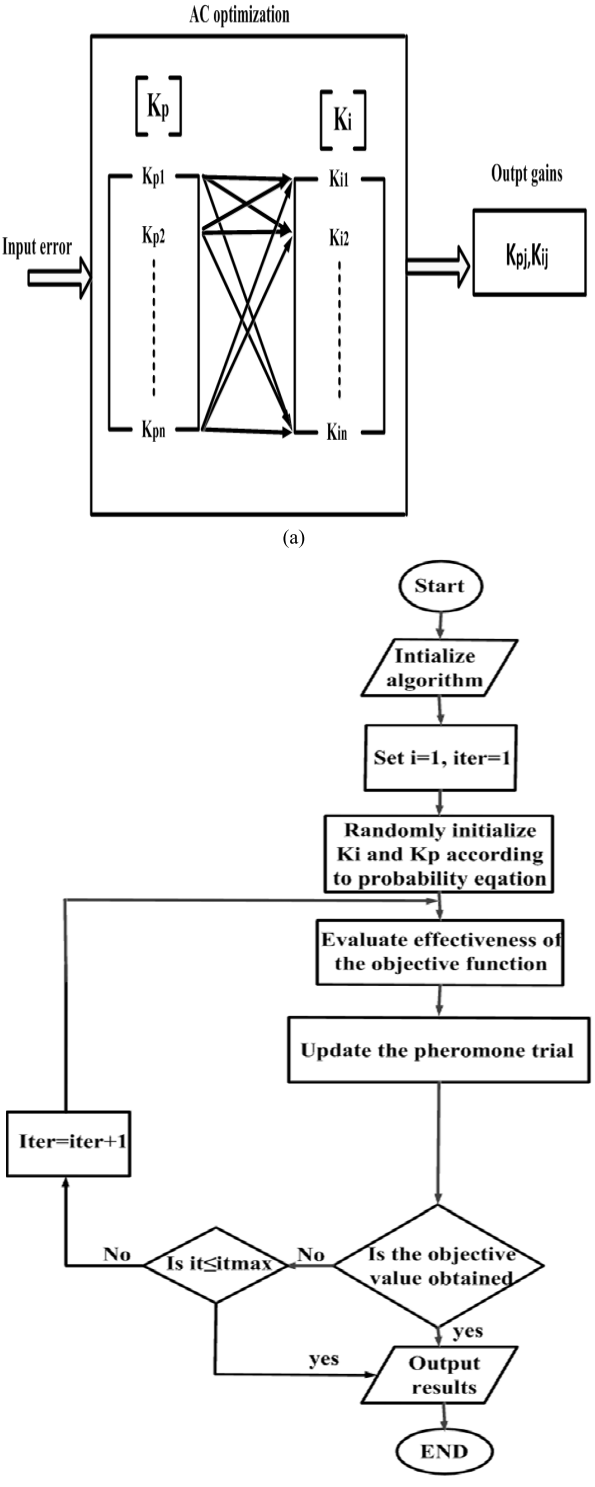

FIGURE 7. (a) ACO as a PI controller. (b) ACO optimization process.

In Figure 7.a, it can be shown that there is a combined set of K_i and K_p which forms a node (cite) at which the ant is

looking at the food. In the current study there are 100 nodes through which the ants search to obtain the optimal gains and those nodes are selected among the upper and lower limits of K_i and K_p [36]. The sequential steps in the ACO optimization process to fine tune PI controller are illustrated in the flowchart of Figure 7.b.

D. PI CONTROLLER BASED ON HYBRID ACO-PSO (HPA)

Both ACO and PSO algorithms are formulated through emulating the animal behavior while seeking to find the food. But the implementation procedure is not the same, in ACO technique the ants generate pheromone routes and based on the weight of this pheromone all ants starts to walk through this route towards the food, while PSO procedure is formulated based on the birds memories to update its location through the tribal area. So the PSO algorithm provides a vast search plan to determine the optimal swarm location and the ACO technique searches the optimal solution around the global optimum location. To achieve fast reach to the optimal global position with less number of iterations, the hybrid ACO-PSO (HPA) technique is used. The HPA was primarily presented in [37], [38]. During the implementation procedure of the HPA technique, the optimal solutions acquired by PSO (P^{gbest}) and ACO (X^{gbest}) are compared at each iteration, then both the pheromone trail and the bird's velocity and position are updated based on the reached optimal solution. Since the HPA algorithm depends on the main principles of both the PSO and ACO, the following relationships describe the HPA implementation stages:

$$\begin{aligned} &If\ F(P^{gbest}) \leq F(X^{gbest}) \\ &X^{gbest} = P^{gbest} \\ &Else \\ &P^{gbest} = X^{gbest} \end{aligned} \tag{15}$$

The following flowchart outlines the implementation procedure of the HPA technique used for enhancing the performance of PI controllers which streamlines the STATCOM dynamic behavior. Figure 8 illustrates the HPA technique.

E. OBJECTIVE FUNCTION OF OPTIMIZATION TECHNIQUES

It is clear that, the classical tuning methods applied for PI controller to obtain best value of integral and proportional gains can be performed using trial and error based expert system (ES). The expert controller contains the knowledge base of tuning the controller and takes several iterations until the best values for PI parameters are obtained. This means more time, regarding system contingency conditions. From this context the optimization techniques are modified and reformulated to generate precise and proper PI controller gains according to specific constraints. The time rate for solving the procedure of the proposed methods is shown in Figure 9. From this figure and during startup time the classical method

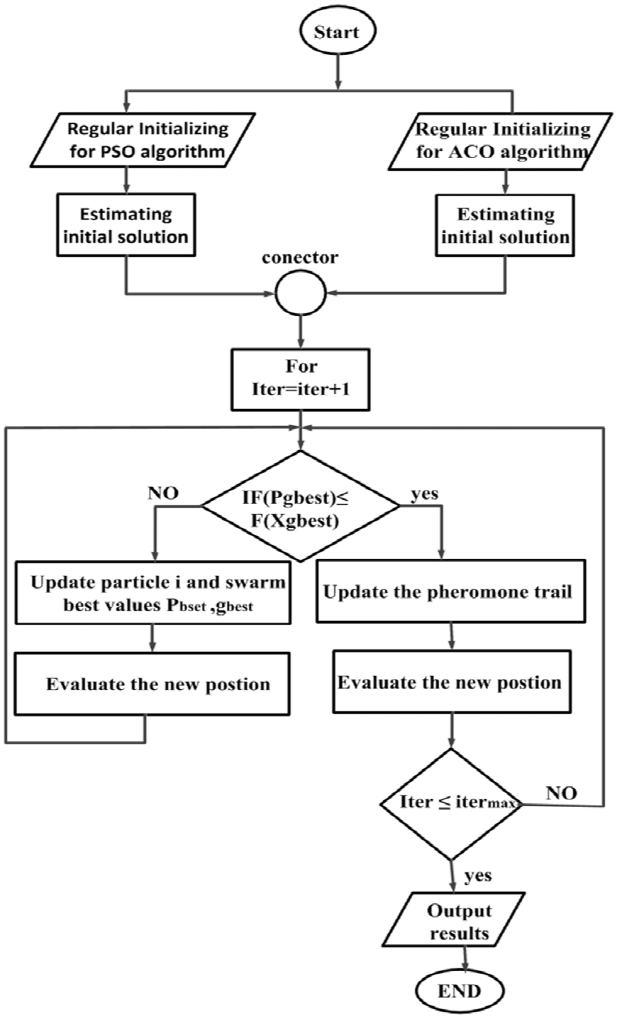

FIGURE 8. Implementation procedure for the HPA process.

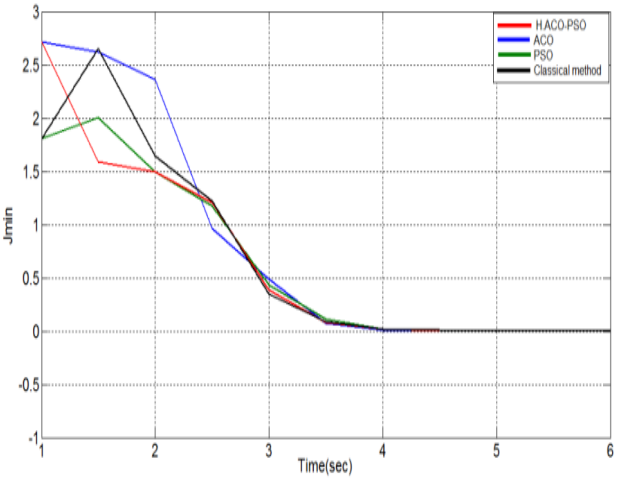

FIGURE 9. Time rate for executing the proposed procedures.

shows divergence which lead to increase the startup time and may lead to make this method get stuck around this value. On the other hand the metaheuristic methods show simple

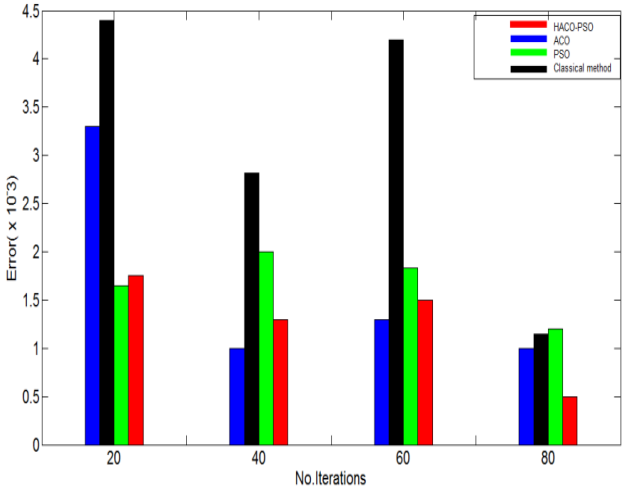

FIGURE 10. Error percentage for the objective value.

TABLE 1. Parameters of PSO algorithm.

PSO parameters	Values
Swarm size	20
Maximum iteration number	80
$c_1 = c_2$	2
ω	0.5
omega_min	0.4
omega_max	0.9

TABLE 2. Parameters of ACO algorithm.

ACO parameters	Values
Number of Ants	50
Nodes in each vector	25
Maximum tour	80
Pheromone update coefficient (τ)	0.5
Evaporation rate (ρ)	5
Relative important parameter of node trail intensity (α)	2
Relative important parameter of visibility (β)	6

TABLE 3. PI controller gains for various tuning algorithms.

		Methods			
		Classical tuning	PSO	ACO	Hybrid PSO-ACO
AC PI Voltage regulator	K_p	17	10.5	14.2	16.8
	K_i	2000	1150	1900	2200
AC PI Current regulator	K_p	8	8.75	9.6	10.9
	K_i	50	34.4	47.5	52.5
DC PI Voltage regulator	K_p	0.0015	0.0026	0.0012	0.00145
	K_i	0.08	0.02	0.0286	0.024

ramp down to achieve the objective value. Another major comparative quantity is shown in Figure 10 where the error percentage is lower for the biological methods and is larger for the classical method. The parameters used for both PSO and ACO methods are given in Tables 1 and 2, respectively.

The main incentive for the biological methods is the objective function, where the sequence steps move around a certain target with a specific constant. There are four common equations that employed to represent the objective function. These equations are, integral absolute error (IAE), and the integral time absolute error (ITAE), integral of time multiplied squared error (ITSE), and the integral squared error (ISE). As presented in [25] the dynamic assessment of the cost function procedures was carried out, and it was concluded that the ISE approach has the best performance compared with the other techniques under transient operating conditions. Nevertheless, in the current study the ITAE function is activated to achieve the targets, which are minimum overshoot points and lower settling time. The ITAE function is specified by,

$$ITAE = \sum_{i=1}^{n} t\,(i) * abs(error\,(i)) \tag{16}$$

It is well realized that the main task of the STATCOM is to provide the reactive power under various fault states so that the DFIG can keep its operation during this fault condition. So the cost function here is Vpcc ≥ 10% of its nominal value.

From Figure 4, it can be noticed that there are three PI controllers which are used to regulate the STATCOM electrical dynamics. These controllers are the AC PI voltage controller, AC PI current controller and the DC PI voltage controller. So The ITAE function is employed, where the target here is to minimize the cost function (J) accompanied with the following constraint.

For the AC voltage regulator

$$J = \sum_{i=1}^{n} t\,(i) * abs(V_{ac_{ref}} - V_{ac_{meas}}(i)) \tag{17}$$

With the constraint of

$$12 \le Kp \le 22, \quad 1500 \le Ki \le 2500$$

For the AC current regulator

$$J = \sum_{i=1}^{n} t\,(i) * abs(i_{ac_{ref}} - i_{ac_{meas}}(i)) \tag{18}$$

With the constraint of

$$4 \le Kp \le 12, \quad 44 \le Ki \le 66$$

For the DC voltage regulator

$$J = \sum_{i=1}^{n} t\,(i) * abs(V_{dc_{ref}} - V_{dc_{meas}}(i)) \tag{19}$$

With the constraint of

$$0.0005 \le Kp \le 0.0015, \quad 0.02 \le Ki \le 0.045$$

Table 3 addresses the different values of PI controller gains using different tuning algorithms.

V. RESULTS AND DISCUSSION

For testing the performance of different PI parameters tuning techniques used with the system shown in Figure 1, a Matlab/Simulink software is utilized. The system's data are presented in Table 8. The clear function of the STATCOM is to relieve the effect of voltage sag across the power lines near bus *B1* via presenting the proper LVRT action. The control methods introduced in this paper are employed to maintain

TABLE 4. Shows a review for international grid codes for WTs-LVRT.

Countries	Fault period		After fault clearance	
	$V_{min}(pu)$	$T_{max}(sec)$	$V_{min}(pu)$	$T_{max}(sec)$
Australia	0.0	0.1	0.7	2
Canada	0.0	0.15	0.85	1
Denmark	0.2	0.5	0.9	1.5
German	0.0	0.15	0.9	1.5
Ireland	0.15	0.625	0.9	3
New Zealand	0.0	0.2	0.6	1
Spain	0.0	0.15	0.85	1
UK	0.15	0.14	0.8	1.2
USA (FERC)	0.15	0.625	0.9	3
USA (WECC)	0.0	0.15	0.9	1.75

the wind farm following the grid code requirement besides improving the power quality quantities. Table 4 gives a summary of international grid code requirements. The dynamic response from the proposed tunning techniques mentioned earlier has been evaluated under three different fault types, the three phases, the double phase and the single line fault. All faults last for 100 ms within which the STATCOM's operation is actuated to provide the wind-turbine DFIG with the necessary magnetization required to keep track with the desired grid codes. A detailed comparison between the different tuning techniques is reported in Table 5 where the distinguished values are the maximum overshoot (MOS), maximum undershoots points (MUS) and the settling time (T_s) for power quality values (voltage and currents) at buses *B1*, *B2*, and V_{dc} (volt) of the DFIG rotor side converter. This is in addition to the active and reactive powers recovery time and responses for the WT-DFIG are investigated, and the rotor mechanical speed (ω_r) is terminated too.

A. SYMMETRICAL THREE PHASE FAULT

Figure 11 illustrates the dynamic behavior of the system for a three phase fault applied at a near point to the bus collector (*B1*). During the fault interval, the terminals of the rotor side converter are connected to crowbar resistances collection so as to prevent the excessive rotor current, while at the same time the STATCOM is providing the necessary reactive power to the DFIG to avoid the disconnection of the wind farm from the utility grid. At bus *B1* the voltage level increases to more than 13% of its rated value. The performance of the PI regulators, based FUZZY regulators, based PSO algorithm, based ACO method and based HPA method have been shown in figure 11(a), 11(b), 11(c), 11(d) and 11(e) respectively. A comparison between the proposed methods utilized for tuning the STATCOM PI controller is summarized in Table 5.

B. LINE TO LINE TO GTOUND FAULT

As shown in Figure 12, a double line to ground fault occurs at 1.2 sec and lasts for 100 msec within which the operation of the STATCOM is actuated trying to prevent the negative sequence currents from spreading to the utility grid by injecting a reactive current beside decreasing the mechanical stress that the shaft of the DFIG-WT exposes. The figure shows the performance of the different techniques which have been applied in this paper; (a) using PI regulators. (b) using FUZZY regulators. (c) using PSO algorithm.(d) using ACO method.(e) using HPA method. As stated, the demonstration of the proposed techniques is shown in Table 5.

From Table 5 it is clear that both FUZZY method and the meta heuristic methods (PSO, ACO, HPA) have better dynamic performance and better power quality than the regular PI method, however the designing of FUZZY system needs for gathering more information from the expert system beside testing the system before using it to make sure that it does perfectly, but the biological methods can adapt itself to obtain the proper gains that drives the STATCOM without gathering or testing the system just by using some constraints and objective function which lead to save time and effort beside providing better dynamic response during transient conditions.

C. SINGLE LINE TO GROUND FAULT

The final fault condition investigated in this paper is the single line to ground fault. During this fault type un-symmetrical components are generated causing unbalanced voltage and currents, so the STATCOM is activated to mitigate the effect of the negative sequential components to spread in the system power lines as shown in Figure 13. Figure 13 illustrates a comprehensive comparison between the dynamic performance under single line to ground fault using different control methods; (a) using PI regulators. (b) using FUZZY regulators. (c) using PSO algorithm.(d) using ACO method.(e) using HPA method.

According to the data shown in Table 4, the grid code states that the voltage level of wind turbine generation system has to be located in a range between zero and about 20% of its rated value under three phase faults for definite periods according to the national grid data provided by each country, so from the results in Figure 11, it can be noticed that the voltage level for three phase fault stays at 13% of rated voltage value at bus *B1* and switches to 85% of its rated at *B2*. Meanwhile, during asymmetrical faults intervals the voltage level exhibits a value of 30% of its rated at *B1* and switches to 93 % of its rated at *B2*. From the illustrated results, the voltage recovers to its rated after 2.5 cycles for 3-phase faults and after 2 cycles for both the 2-phase fault and the 1-phase fault, this is achieved without using any resistors connected to the stator terminals as presented in [13], [17] and presents better dynamic behaviors compared with the results obtained in [16].

Since the most serious problem that the WT-DFIG would face is the deep faults that occur at the nearest bus to the DFIG. However, using STATCOM accompanied with a proper control scheme enhances the dynamic response

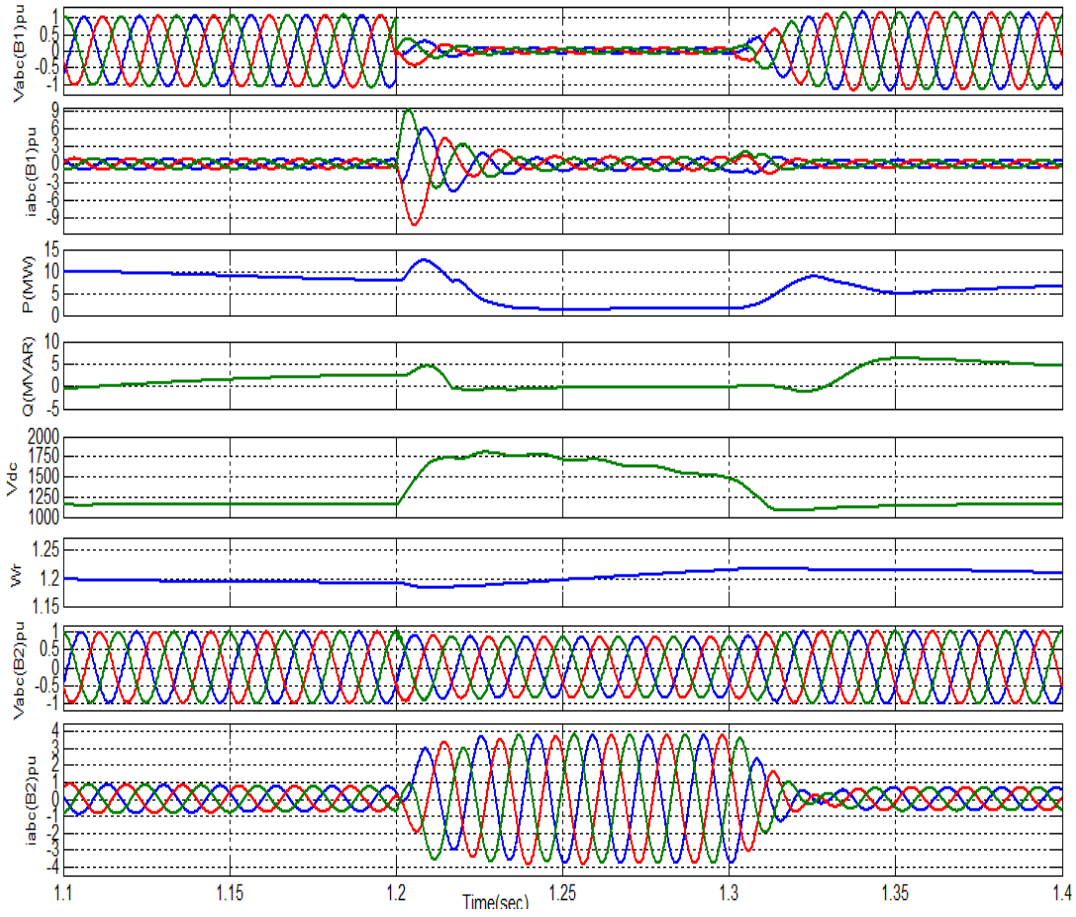

(a)

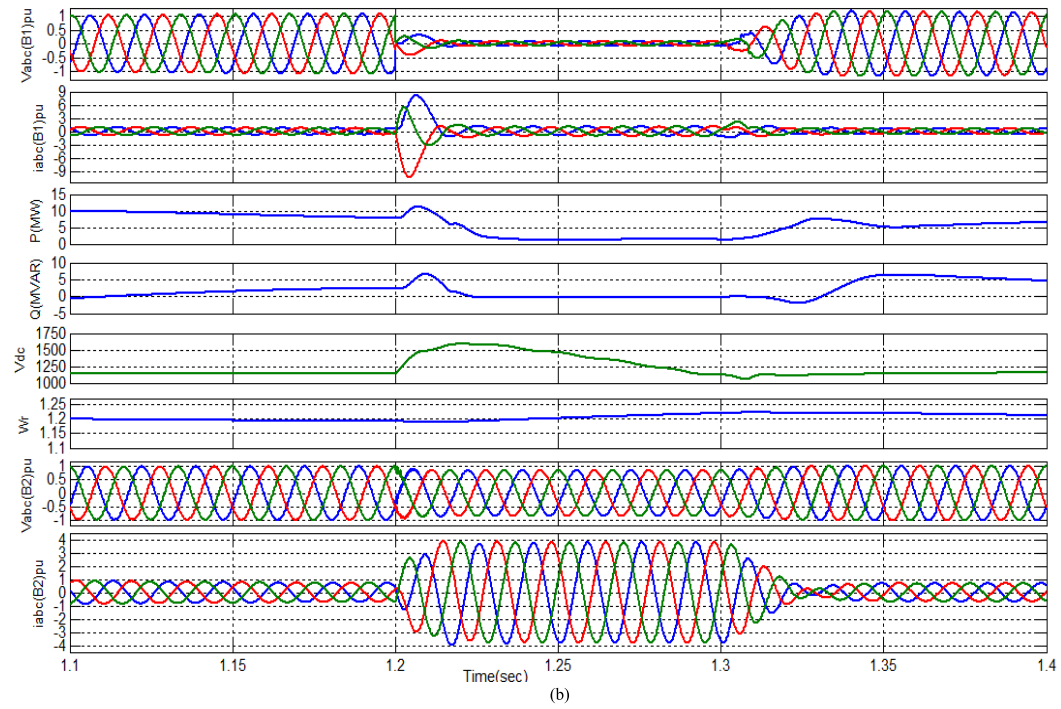

(b)

FIGURE 11. System dynamic behavior under three phase fault (a) usingPI regulators. (b) using FUZZY regulators. (c) using PSO algorithm. (d) using ACO method. (e) using HPA method.

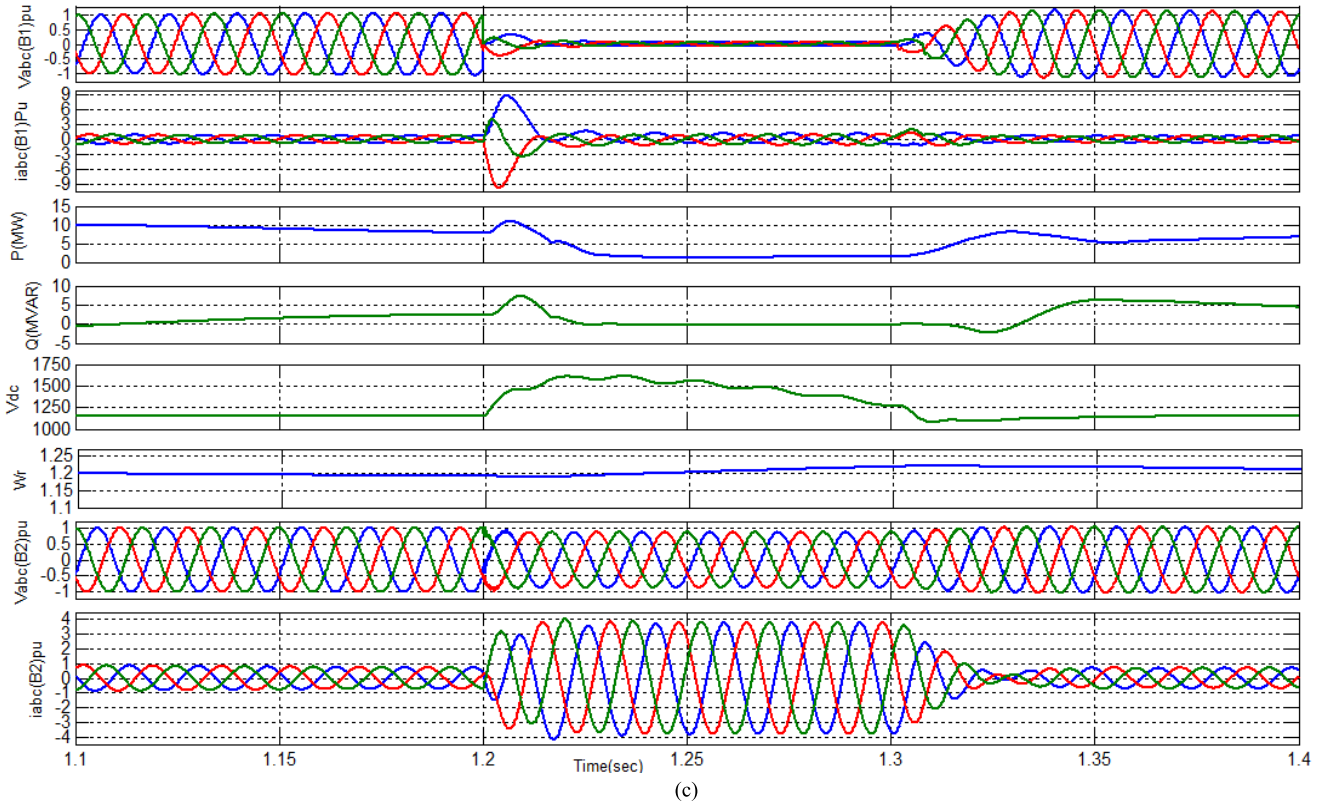

(c)

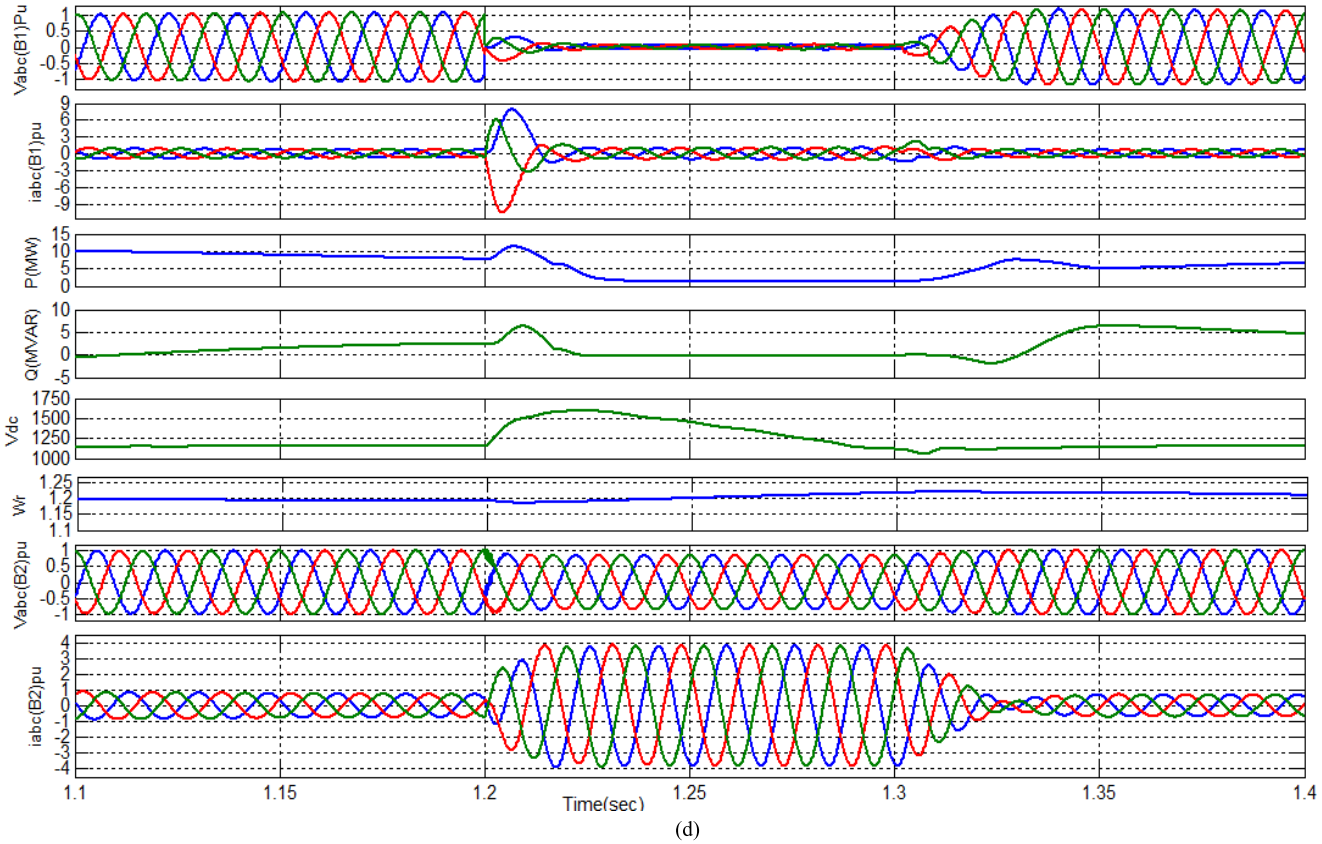

(d)

FIGURE 11. *(Continued)* **System dynamic behavior under three phase fault (a) usingPI regulators. (b) using FUZZY regulators. (c) using PSO algorithm. (d) using ACO method. (e) using HPA method.**

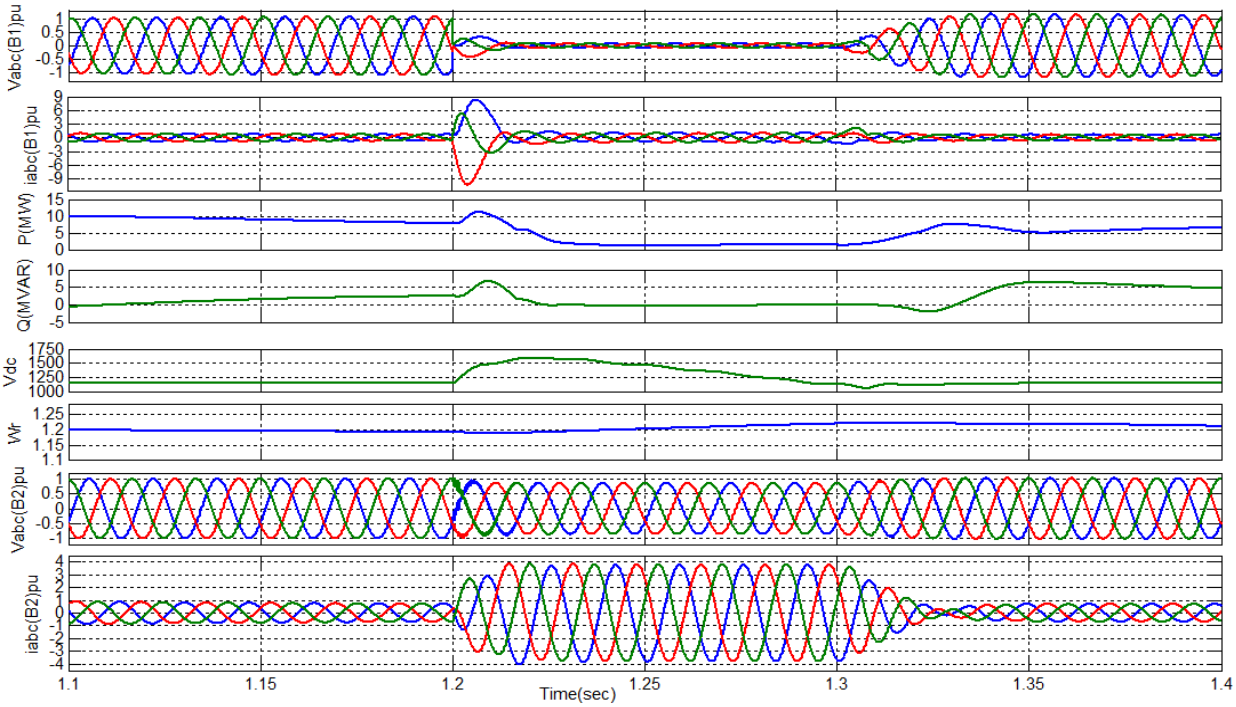

(e)

FIGURE 11. *(Continued)* **System dynamic behavior under three phase fault (a) usingPI regulators. (b) using FUZZY regulators. (c) using PSO algorithm. (d) using ACO method. (e) using HPA method.**

TABLE 5. **Numerical summary of results obtained.**

			Methods				
Faults	**Measured values**	**Transient points**	**PI**	**FUZZY**	**PSO**	**ACO**	**PSO-ACO**
1- Φ-G Fault	V_{abc}(B1)	MOS	0.768R	0.6Y	0.58Y	0.62Y	0.6Y
		MUS	-1R	-0.58	-0.5G	-0.6G	-0.6G
		Ts(sec)	0.035	0.038	0.038	0.035	0.035
	i_{abc}(B1)	MOS	9.4Y	9.5Y	9.56Y	9.5Y	9.5Y
		MUS	-7.16Y	-2.2R	-2G	-2.4Y	-2.3R
		Ts(sec)	0.03	0.025	0.025	0.03	0.029
	V_{dc}	MOS	1220.8	1350	1378	1266.8	1315
		MUS	1108	1072	1062	1093.18	1063.28
		Ts(sec)	0.04	0.048	0.48	0.045	0.044
2- Φ-G Fault	V_{abc}(B1)	MOS	0.5Y	0.43Y	0.4Y	0.44Y	0.6Y
		MUS	-0.55G	-0.48R	-0.45R	-0.5R	-0.6G
		Ts(sec)	0.035	0.035	0.033	0.035	0.035
	i_{abc}(B1)	MOS	9.6Y	10Y	10Y	10Y	9.5Y
		MUS	-9.3R	-9,25R	-8.87R	-9.4R	-2.3R
		Ts(sec)	0.029	0.025	0.022	0.03	0.029
	V_{dc}	MOS	1460	1350	1348	1346	1315
		MUS	1070	1078	1069	1080	1063.28
		Ts(sec)	0.06	0.042	0.045	0.044	0.044
3-Φ Fault	V_{abc}(B1)	MOS	0.37G	0.31Y	0.32Y	0.31Y	0.32Y
		MUS	-0.42R	-0.4R	-0.4R	-0.4R	-0.4R
		Ts(sec)	0.038	0.038	0.038	0.035	0.035
	i_{abc}(B1)	MOS	9.2G	8Y	9Y	8Y	8.4Y
		MUS	-10R	-10R	-10R	-10.15R	-10.29R
		Ts(sec)	0.029	0.028	0.025	0.038	0.029
	V_{dc}	MOS	1800	1378	1616	1590	1588.8
		MUS	1072.8	1062	1080	1054	1053
		Ts(sec)	0.08	0.48	0.05	0.049	0.049

R: represents the red phase, G represents the green phase, B : represents the blue phase

of the system under the grid fault conditions. It is clearly noticed that the current signals at *B1* as shown in Figure 11, are almost recovered its pre-fault nominal value during the 3-phase faults. On the other hand for asymmetrical faults the STATCOM injects the reactive power needed to compensate the negative sequence currents, hence the grid currents

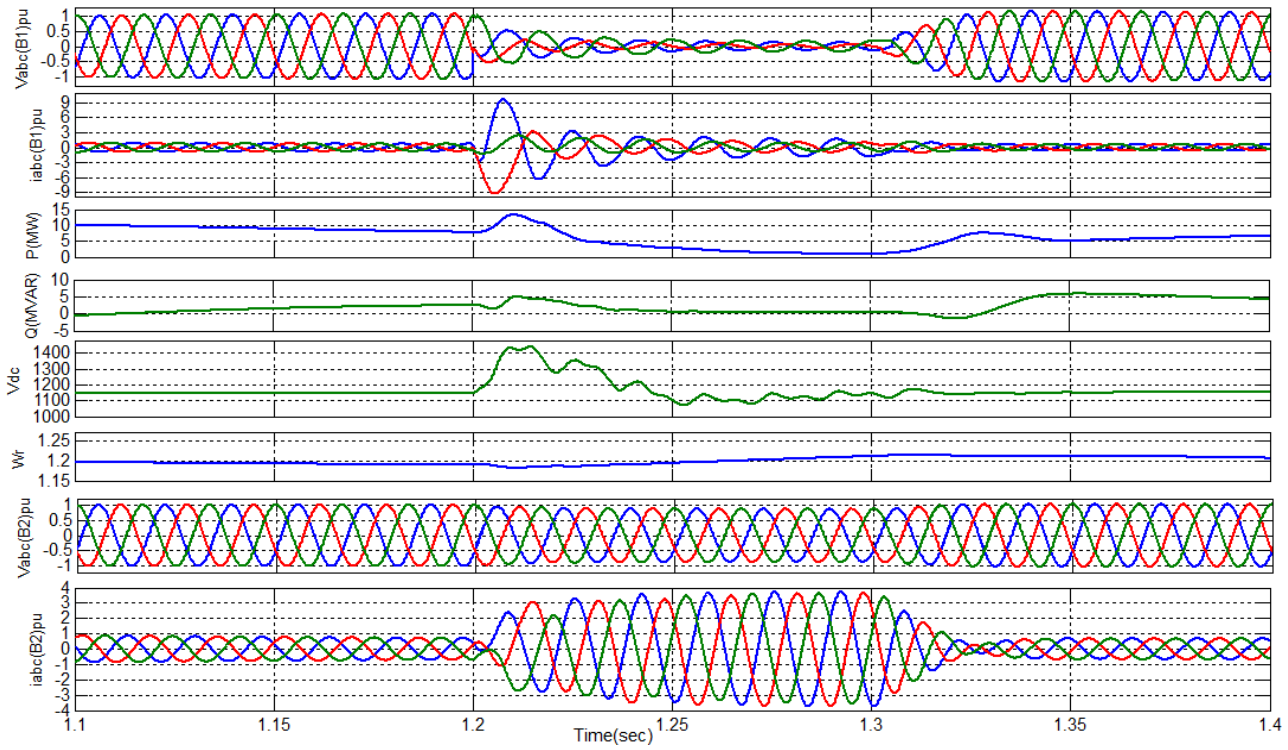

(a)

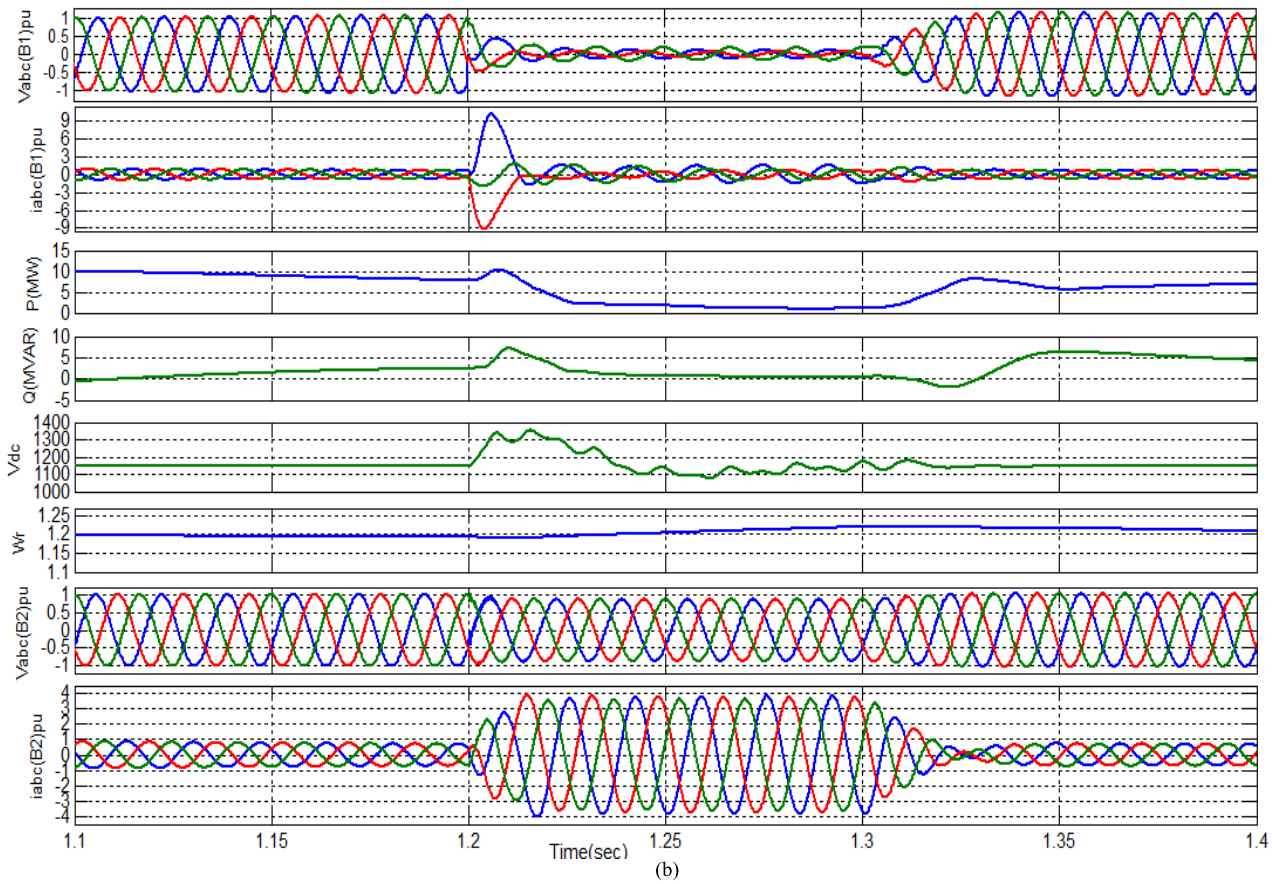

(b)

FIGURE 12. Dynamic performance under double line to ground fault (a) using PI regulators. (b) using FUZZY regulators. (c) using PSO algorithm. (d) using ACO method. (e) using HPA method.

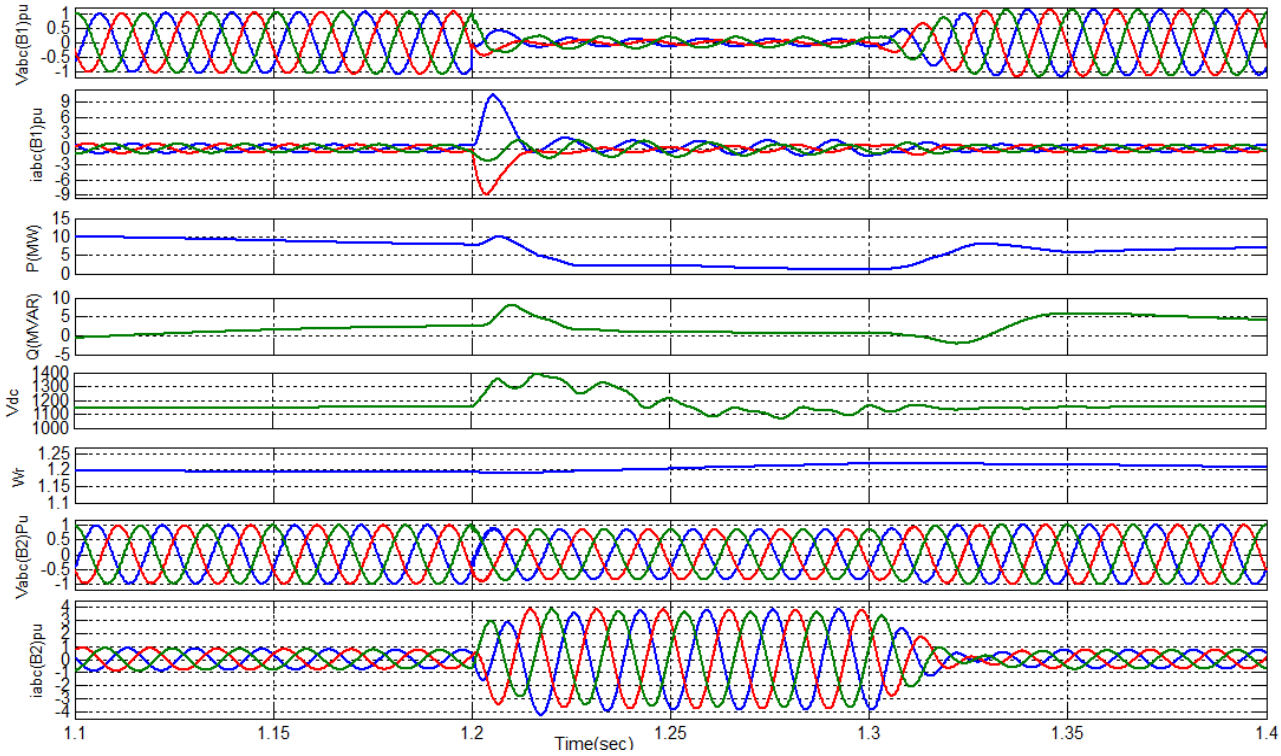

(c)

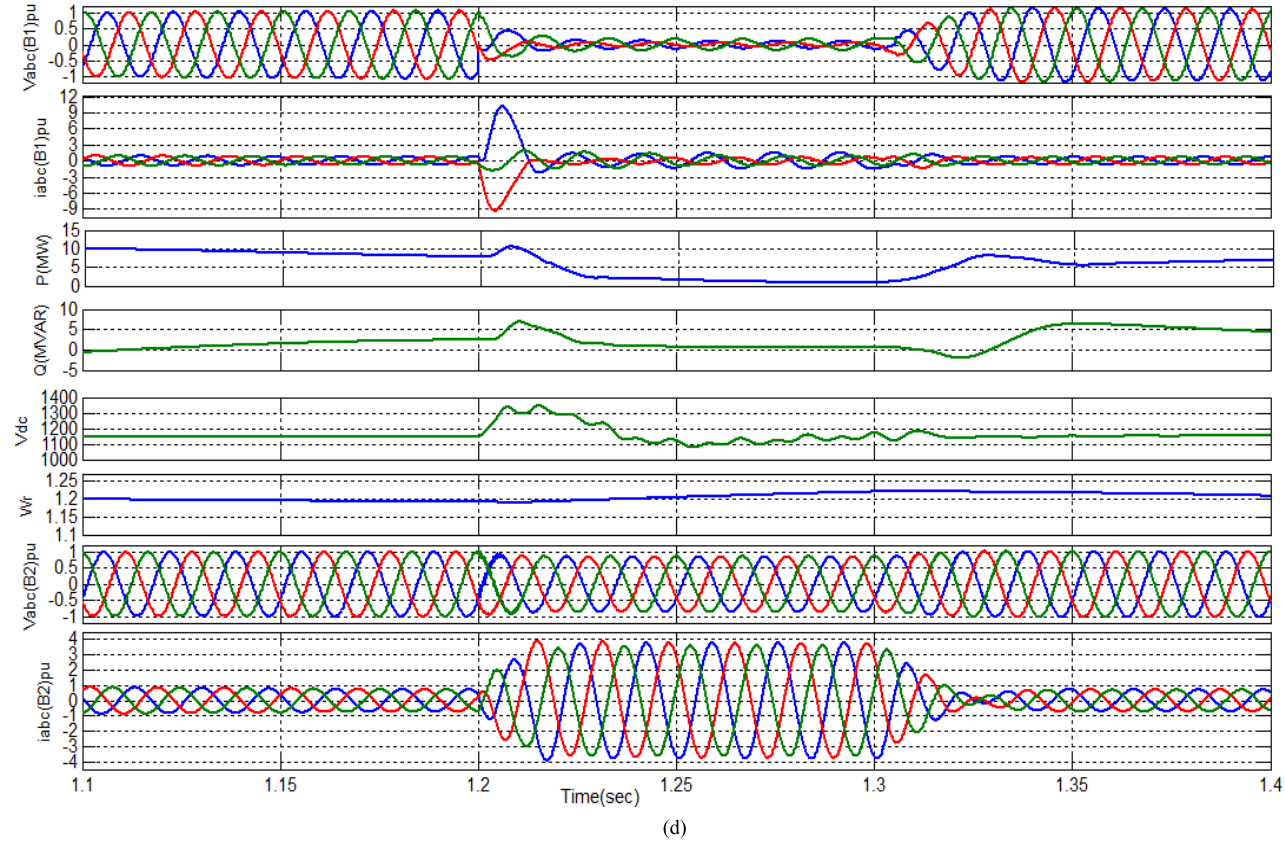

(d)

FIGURE 12. *(Continued)* **Dynamic performance under double line to ground fault (a) using PI regulators. (b) using FUZZY regulators. (c) using PSO algorithm. (d) using ACO method. (e) using HPA method.**

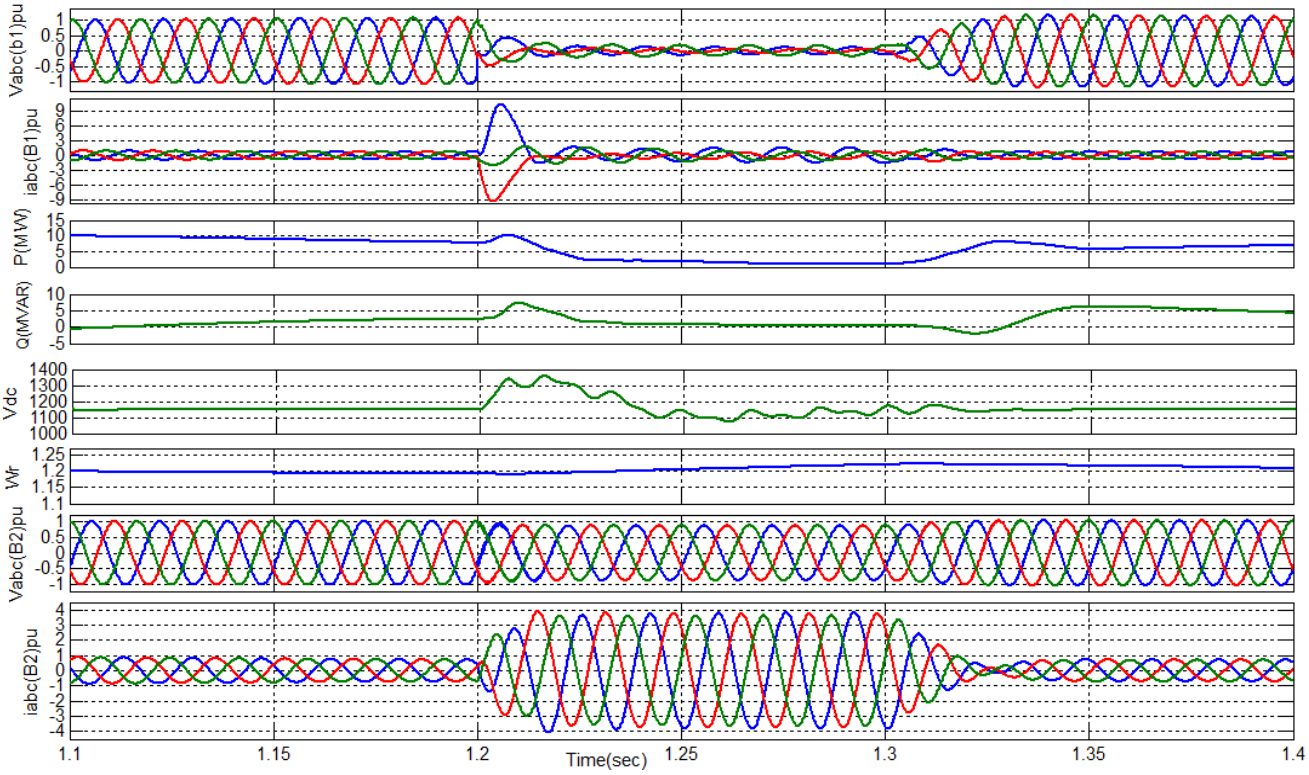

(e)

FIGURE 12. *(Continued)* **Dynamic performance under double line to ground fault (a) using PI regulators. (b) using FUZZY regulators. (c) using PSO algorithm. (d) using ACO method. (e) using HPA method.**

appears almost balanced currents. The grid currents take about 1.5 cycle to recover its nominal value during the post-fault interval for all fault cases.

From results shown, the most severe case that the DC-link voltage of the rotor side converter encounters is in the time of the three phase fault where the V_{dc} presents a value of 1.5 of its nominal value which much better than other results obtained in [12].The value of V_{dc} obtained in this paper ($1.5V_{dc}$ rated) is higher than the value the DC-link reaches in [16] which is 1.25 of the nominal, however the dynamic system response under the severe faults conditions is much better because of the ability of the STATCOM in limiting the peak value to be within the safe permissible range, besides providing fast recovery time after clearing the fault. For the 2 – phase un-balanced severe faults, the maximum value of the DC-link voltage is 1.3 of its rated value with pulsation between +50 and-50. While for 1-phase faults the peak o the DC-link voltage is 1.23 of its rated value and the pulsation looks like the double line fault.

Alongside illustrating the components of power quality at buses *B1* and *B2*, there is a remarkable issue related to the shaft of the DFIG-WT system during the severe faults, and this issue is the increased mechanical stress. The wind turbine shaft accelerates in an attempt to rapidly restore the voltage and currents of the DFIG which increases the mechanical stress on the turbine shaft. Speeding up the DFIG's speed during the un-balanced faults (single line fault and double line fault) is a critical situation because of the resultant torque pulsations generated from the unsymmetrical component which appear in the grid lines. In the following figures the DFIG's speed rises from 1.2 pu up to 1.25 pu within the period of 3-phase faults, and almost constant with little fluctuation for the asymmetrical faults.

D. ACTIVE POWER RECOVERING

The regulation of active and reactive power is considered as a big challenge to the countries which possess large production of electricity from wind energy plants. For this reason, the grid requirements force the large WPPs to ensure active and reactive power control within and after the fault occurrence to enhance system stability. It can be observed from the figures that there is no discontinuity for the active power during various fault conditions. Moreover, thanks to reactive power regulation during the fault period, the active power recovers very quickly to its pre-fault value which agrees with the grid code terms. Table 6 shows the recovered values of active power after distinguishing the fault for the five algorithms described earlier.

E. ANALYSIS OF TOTAL HARMONIC DISTORTION (THD)

Although harmonics problems are not as widespread as the RMS voltage variation, the harmonic distortion has an

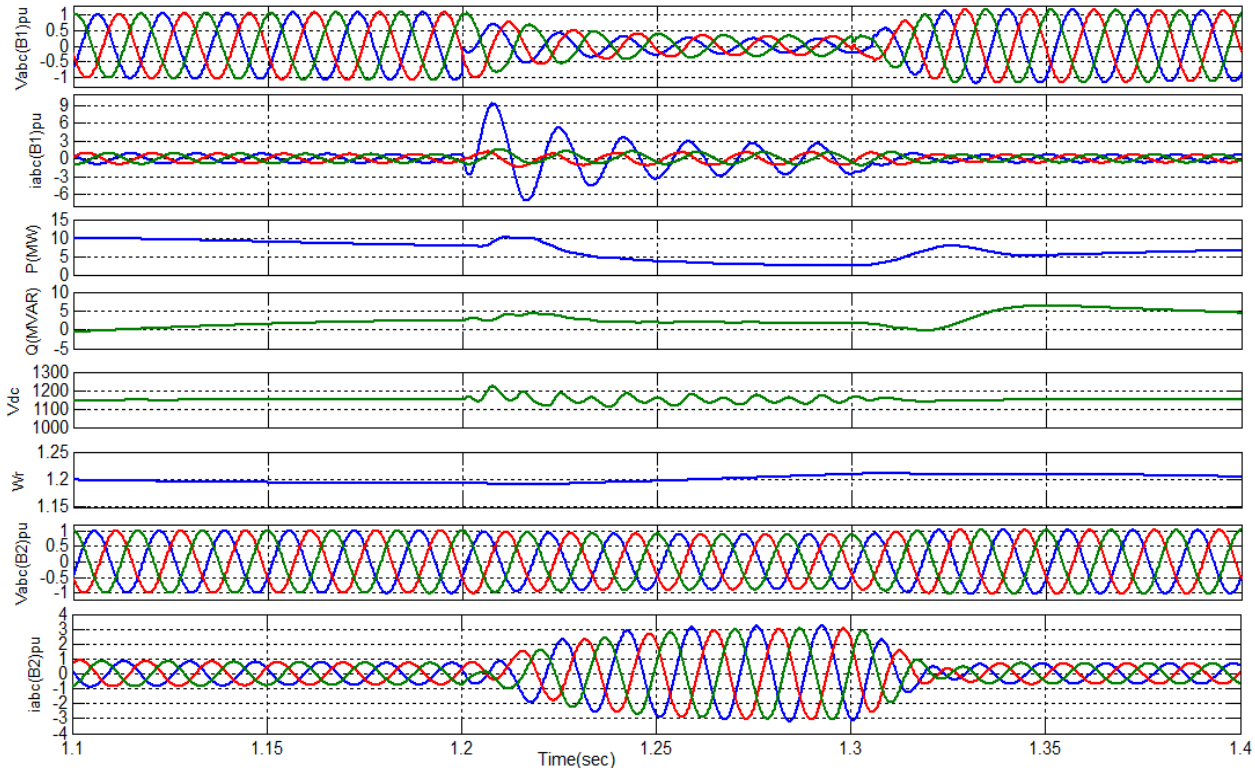

(a)

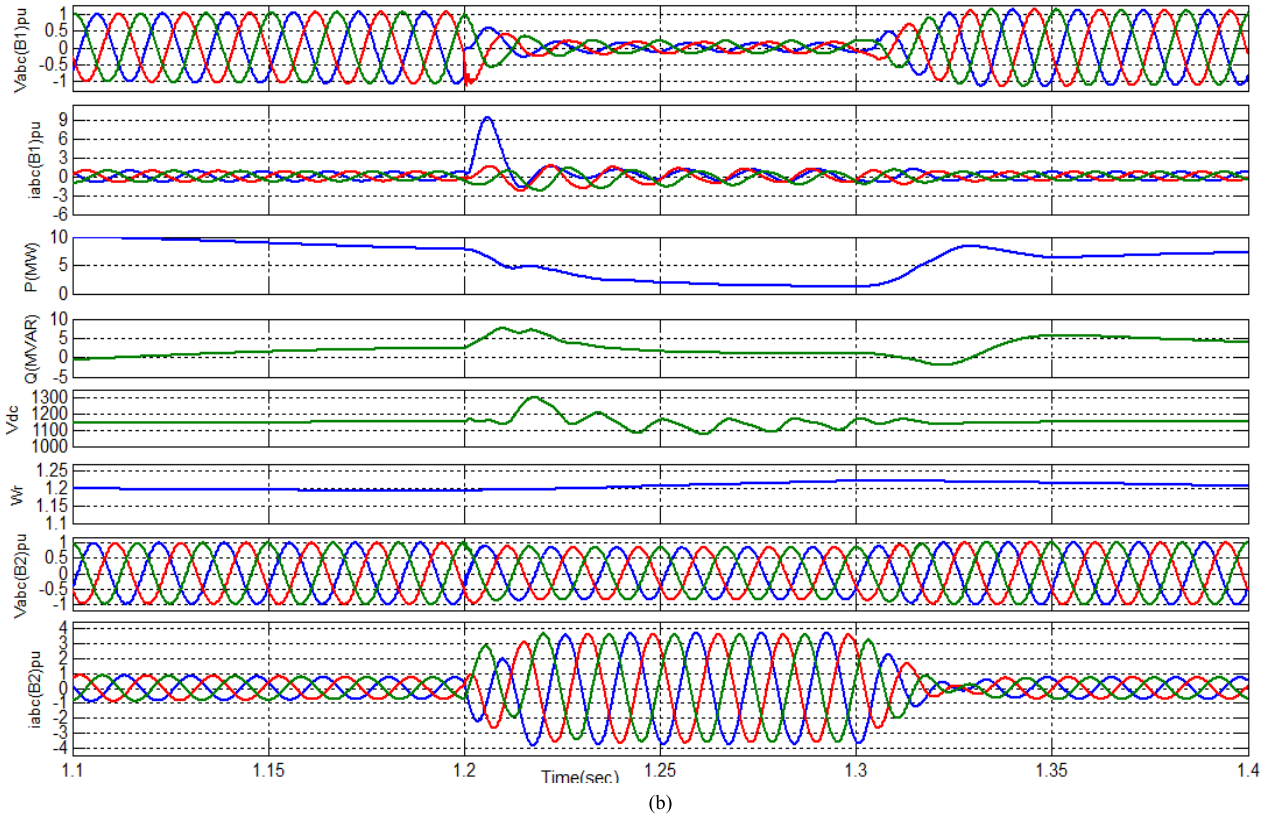

(b)

FIGURE 13. Dynamic performance under single line to ground fault (a) using PI regulators. (b) using FUZZY regulators. (c) using PSO algorithm. (d) using ACO method. (e) using HPA method.

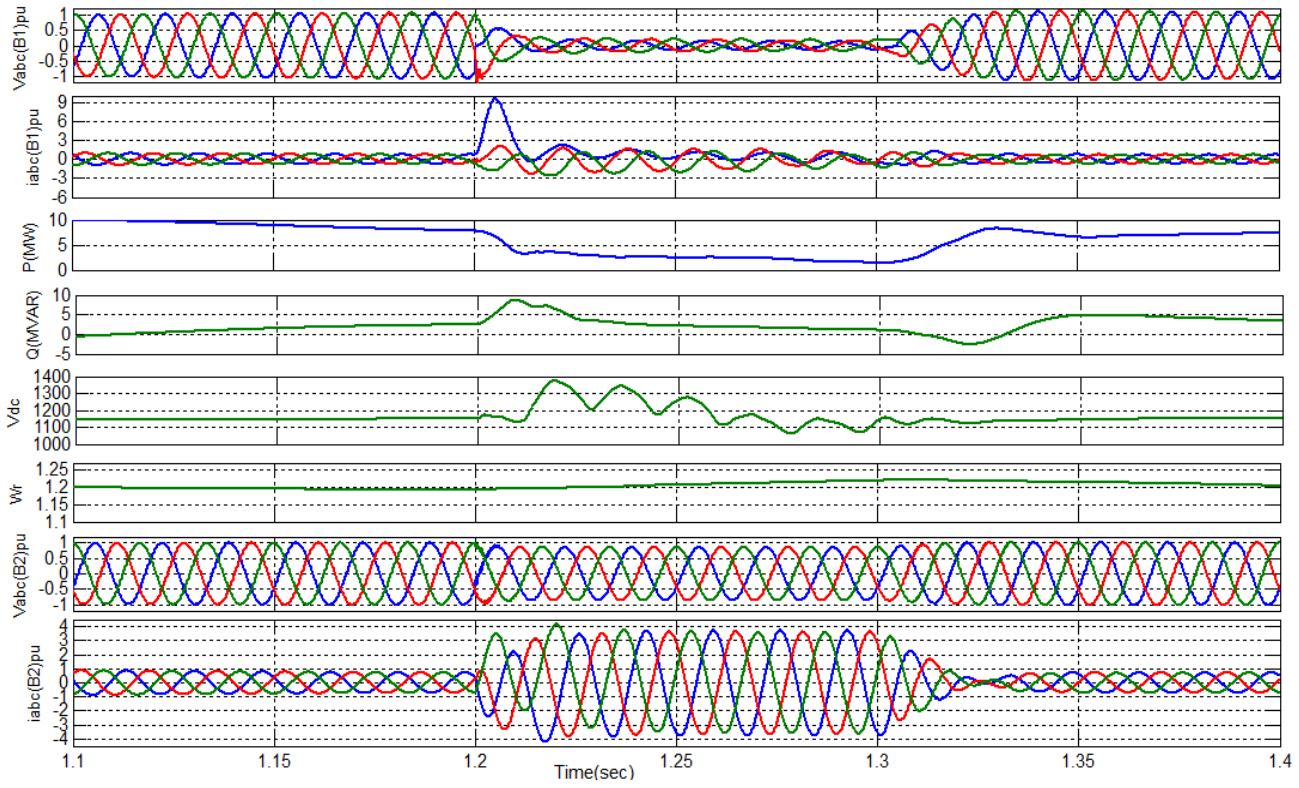

(c)

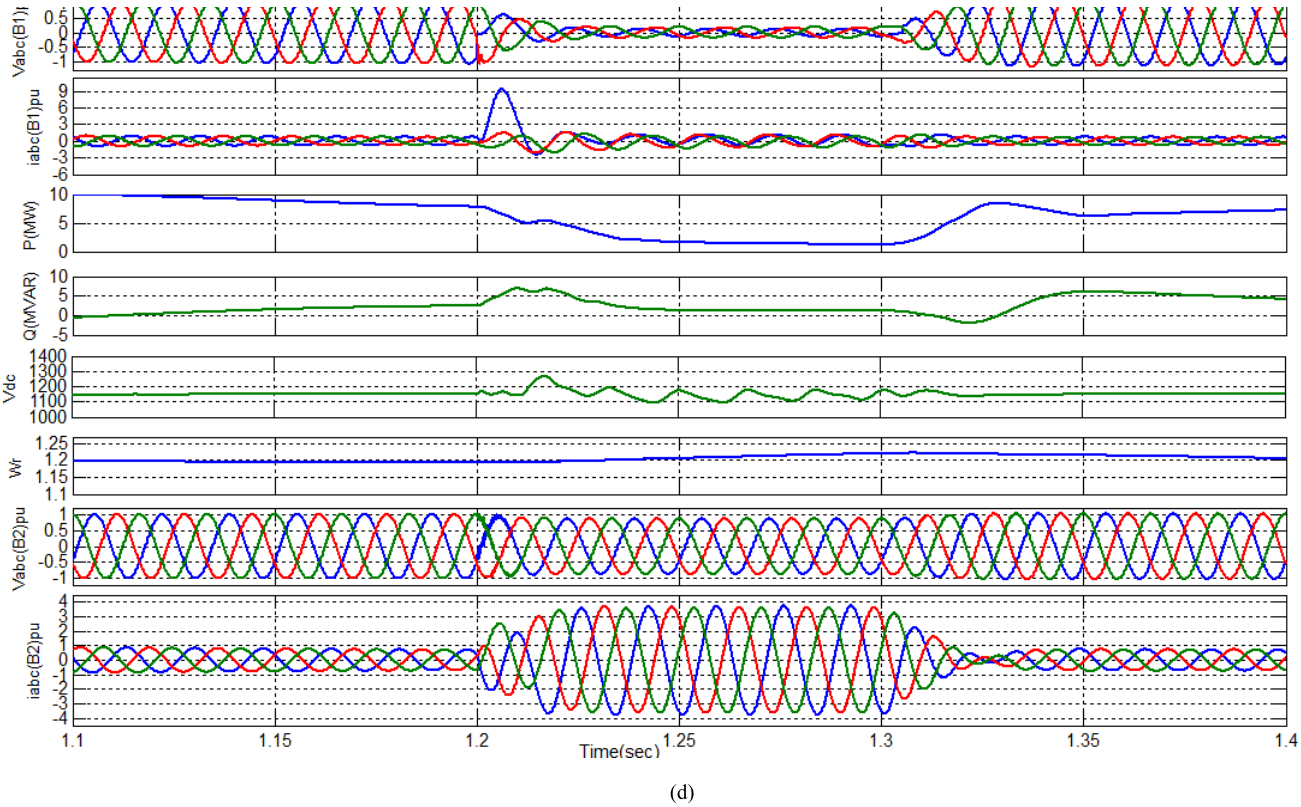

(d)

FIGURE 13. *(Continued)* **Dynamic performance under single line to ground fault (a) using PI regulators. (b) using FUZZY regulators. (c) using PSO algorithm. (d) using ACO method. (e) using HPA method.**

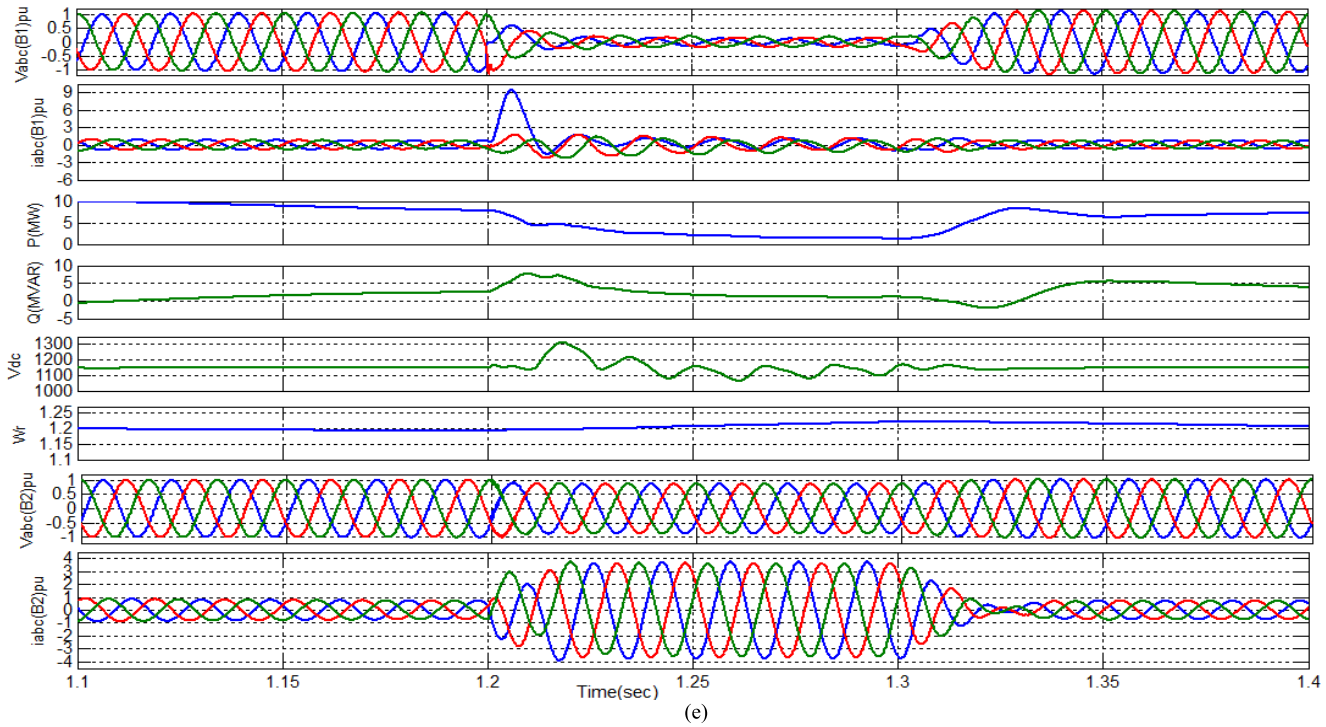

FIGURE 13. *(Continued)* **Dynamic performance under single line to ground fault (a) using PI regulators. (b) using FUZZY regulators. (c) using PSO algorithm. (d) using ACO method. (e) using HPA method.**

TABLE 6. **Active and reactive power recovery after fault clearance.**

			Methods				
			PI	FUZZY	PSO	ACO	PSO-ACO
P(MW)	1- Φ-G fault	At t=1.3 sec	5	6.2	6.5	6.2	6.35
		At t=1.375 sec	6	6.85	7	6.8	6.8
		At t =1.3 sec	6.6	7.25	7.4	7.2	7.26
	2- Φ-G fault	At t=1.3 sec	5	5.7	5.75	5.6	5.7
		At t=1.375 sec	6	6.5	6.5	6.3	6.5
		At t =1.3 sec	6.6	6.95	7.01	7	7
	3- Φ-G fault	At t=1.3 sec	5	5.1	5.4	5	5.15
		At t=1.375 sec	6	6	6	5.8	5.8
		At t =1.3 sec	6.6	6.5	6.7	6.5	6.6
Q(Mvar)	1- Φ-G fault	At t=1.3 sec	6.27	5.6	4.8	6	5.52
		At t=1.375 sec	5	4.8	4	5.2	4.8
		At t =1.3 sec	4.4	3.9	3.35	4	3.8
	2- Φ-G fault	At t=1.3 sec	5.82	6.2	5.9	6.28	6.2
		At t=1.375 sec	5.2	5.3	5	5.5	5.35
		At t =1.3 sec	4.25	4.32	4	4.4	4.3
	3- Φ-G fault	At t=1.3 sec	6.15	6.31	6.2	6.5	6.26
		At t=1.375 sec	5.5	5.6	5.4	5.7	5.56
		At t =1.3 sec	4.4	4.6	4.4	4.6	4.6

impact effect on the power system components such as casing additional heating for cables, transformers and motors, and produces interface to the communication and electronic circuits. Therefore, the THD for the voltage and currents at *B1* are summarized in Table 7 to cmpare between the different algorithms. From Table 7 both the biological algorithms (PSO, ACO, and HPA) and the FUZZY algorithms have less impact on the power system than regular PI method.

TABLE 7. Shows the THD as a percentage of the fundamental value.

		PI	FUZZY	PSO	ACO	PSO-ACO
V_{abc}(B1)	1- Φ-G fault	6.73%	7.15%	7.16%	7.12%	7.16%
	2- Φ-G fault	7.22%	7.12%	7.18%	7.1%	7.13%
	3- Φ-G fault	7.17%	7.6%	7.38%	7.59%	7.58%
i_{abc}(B1)	1- Φ-G fault	45.85%	18.5%	16.38%	18.96%	18.42%
	2- Φ-G fault	35.55%	29.14%	28.48%	29.45%	28.92%
	3- Φ-G fault	25.43%	27.69%	20.85%	28.85%	26.92%

TABLE 8. Data and parameters.

Elements	Parameters	Values
DFIG (Doubly Fed Induction generator)	P (rated active power)	1.5 MW
	V_s (rated stator voltage)	575 volt
	F_s (rated frequency)	60 Hz
	R_s (stator resistance)	0.023 pu
	L_s (stator inductance)	0.18 pu
	R_r (rotor resistance)	0.016 pu
	L_r (rotor inductance)	0.16 pu
	L_m (magnetizing inductance)	2.9 pu
STATCOM (Static Var Compensator)	V (rated voltage)	25 KV
	Q (rated reactive power)	30 MVAR
	V_{dc} (DC link voltage)	5000
	S (rated apparent power)	11MVA
	$V1$ (primary winding voltage)	575 volt
575V/25KV transformer	R_1 (primary resistance)	8.333e-4 pu
	L_1 (primary inductance)	0.025 pu
	$V2$ (secondary winding voltage)	25 KVolt
	R_2 (secondary resistance)	8.333e-4 pu
	L_2 (secondary inductance)	0.025 pu
Transmission line	L (length)	30 Km
	R (resistance)	0.1153 ohm/Km
	L (inductance)	1.053e-3 H/Km
	C (capacitance)	11.33e-9 F/Km
25/120KV	S (rated apparent power)	47 MVA
	$V1$ (primary winding voltage)	25Kvolt
	R_1 (primary resistance)	0.0026667 pu
	L_1 (primary inductance)	0.08 pu
	V_2 (secondary winding voltage)	120 Kvolt
	R_2 (secondary resistance)	0.0026667 pu
	L_2 (secondary inductance)	0.08 pu

VI. CONCLUSION

According to the fault location and the operating conditions of the system, the fault can cause either temporary voltage drop (sag), voltage rise (swells) or complete loose of voltage (interruptions), in addition to large currents flowing from the generators to the point of fault location. In this paper only the voltage sage is investigated. Voltage sage and interruptions are related power quality problem and responsible for tripping of consumers' loads. It is reported that large production plants have been brought to halt by sags of 100ms duration or less, leading to losses of hundreds of thousands of pounds so this kind of problems give the motivation for the development of custom power equipment such as SVC and STATCOM. Since STATCOM is able to provide rapid active and reactive power compensations to power systems, and therefore can be used to provide voltage support and power flow control, increase transient stability and improve power oscillation damping, in this paper the impact effect of STATCOM at PCC where a wind farm exists is investigated under deep disturbances. Five different techniques are applied to tune the PI regulators employed to control the STATCOM performance, classical PI, FUZZY logic, PSO, AC, hybrid PSO-AC, the major points to evaluate the performance of these methods are the overshoot points during the fault occurrence and the settling time for recovering the system to steady state again. It was clear that PI has less performance efficiency than the other techniques, and the biological methods PSO, ACO and hybrid PSO-ACO having the best ever performance than the FUZZY logic. Thus the meta-heuristic methods such as PSO, ACO and HPA can be exploited to realize enhanced dynamic behavior and saving both time and effort in formulating an appropriate methodology which keeps the WT-DFIGs following precisely the grid code necessities.

APPENDIX

See Table 8.

REFERENCES

[1] A. Vitina, S. Lüers, A.-K. Wallasch, V. Berkhout, A. Duffy, B. Cleary, L. I. Husabø, D. E. Weir, R. Lacal-Arántegui, M. Hand, E. Lantz, K. Belyeu, R. H. Wiser, M. Bolinger, and B. Hoen, "IEA wind task 26. Wind technology, cost, and performance trends in Denmark, Germany, Ireland, Norway, the European union, and the united states: 2007–2012," Nat. Renew. Energy Lab., Golden, CO, USA, Tech. Rep. NREL/TP-6A20-64332, Jun. 2015.

[2] G. M. Joselin Herbert, S. Iniyan, and D. Amutha, "A review of technical issues on the development of wind farms," *Renew. Sustain. Energy Rev.*, vol. 32, pp. 619–641, Apr. 2014.

[3] J. Zou, C. Peng, Y. Yan, H. Zheng, and Y. Li, "A survey of dynamic equivalent modeling for wind farm," *Renew. Sustain. Energy Rev.*, vol. 40, pp. 956–963, Dec. 2014.
[4] M. Boutoubat, L. Mokrani, and M. Machmoum, "Control of a wind energy conversion system equipped by a DFIG for active power generation and power quality improvement," *Renew. Energy*, vol. 50, pp. 378–386, Feb. 2013.
[5] A. A. B. M. Zin, H. A. M. Pesaran, A. B. Khairuddin, L. Jahanshaloo, and O. Shariati, "An overview on doubly fed induction generators controls and contributions to wind based electricity generation," *Renew. Sustain. Energy Rev.*, vol. 27, pp. 692–708, Nov. 2013.
[6] H. Geng, X. Xi, and G. Yang, "Small-signal stability of power system integrated with ancillary-controlled large-scale DFIG-based wind farm," *IET Renew. Power Gener.*, vol. 11, no. 8, pp. 1191–1198, Jul. 2017.
[7] M. Mohseni and S. M. Islam, "Review of international grid codes for wind power integration: Diversity, technology and a case for global standard," *Renew. Sustain. Energy Rev.*, vol. 16, no. 6, pp. 3876–3890, Aug. 2012.
[8] J. Ouyang and X. Xiong, "Dynamic behavior of the excitation circuit of a doubly-fed induction generator under a symmetrical voltage drop," *Renew. Energy*, vol. 71, pp. 629–638, Nov. 2014.
[9] T. S. Abuaisha, "General study of the control principles and dynamic fault behaviour of variable-speed wind turbine and wind farm generic models," *Renew. Energy*, vol. 68, pp. 245–254, Aug. 2014.
[10] S. B. Naderi, M. Negnevitsky, A. Jalilian, M. T. Hagh, and K. M. Muttaqi, "Low voltage ride-through enhancement of DFIG-based wind turbine using DC link switchable resistive type fault current limiter," *Int. J. Elect. Power Energy Syst.*, vol. 86, pp. 104–119, Mar. 2017.
[11] J. J. Justo, F. Mwasilu, and J.-W. Jung, "Doubly-fed induction generator based wind turbines: A comprehensive review of fault ride-through strategies," *Renew. Sustain. Energy Rev.*, vol. 45, pp. 447–467, May 2015.
[12] T. D. Vrionis, X. I. Koutiva, and N. A. Vovos, "A genetic algorithm-based low voltage ride-through control strategy for grid connected doubly fed induction wind generators," *IEEE Trans. Power Syst.*, vol. 29, no. 3, pp. 1325–1334, May 2014.
[13] J. Mohammadi, S. Afsharnia, and S. Vaez-Zadeh, "Efficient fault-ride-through control strategy of DFIG-based wind turbines during the grid faults," *Energy Convers. Manage.*, vol. 78, pp. 88–95, Feb. 2014.
[14] W. Guo, L. Xiao, and S. Dai, "Enhancing low-voltage ride-through capability and smoothing output power of DFIG with a superconducting fault-current limiter–magnetic energy storage system," *IEEE Trans. Energy Convers.*, vol. 27, no. 2, pp. 277–295, Jun. 2012.
[15] A. Tilli, C. Conficoni, and A. Hashemi, "An effective control solution for doubly-fed induction generator under harsh balanced and unbalanced voltage sags," *Control Eng. Pract.*, vol. 84, pp. 172–182, Mar. 2019.
[16] D. V. N. Ananth and G. V. Nagesh Kumar, "Fault ride-through enhancement using an enhanced field oriented control technique for converters of grid connected DFIG and STATCOM for different types of faults," *ISA Trans.*, vol. 62, pp. 2–18, May 2016.
[17] D. Ramirez, S. Martinez, F. Blazquez, and C. Carrero, "Use of STATCOM in wind farms with fixed-speed generators for grid code compliance," *Renew. Energy*, vol. 37, no. 1, pp. 202–212, Jan. 2012.
[18] R. Baños, F. Manzano-Agugliaro, F. G. Montoya, C. Gil, A. Alcayde, and J. Gómez, "Optimization methods applied to renewable and sustainable energy: A review," *Renew. Sustain. Energy Rev.*, vol. 15, no. 4, pp. 1753–1766, May 2011.
[19] M. Eremia and L. Chen-Ching. *Static Synchronous Series Compensator (SSSC)*. Hoboken, NJ, USA: Wiley, 2016.
[20] L. Gidwani, H. Tiwari, and R. C. Bansal, "Improving power quality of wind energy conversion system with unconventional power electronic interface," *Int. J. Electr. Power Energy Syst.*, vol. 44, no. 1, pp. 445–453, Jan. 2013.
[21] L. Wang, C.-H. Chang, B.-L. Kuan, and A. V. Prokhorov, "Stability improvement of a two-area power system connected with an integrated onshore and offshore wind farm using a STATCOM," *IEEE Trans. Ind. Appl.*, vol. 53, no. 2, pp. 867–877, Mar./Apr. 2017.
[22] A. Movahedi, A. H. Niasar, and G. B. Gharehpetian, "Designing SSSC, TCSC, and STATCOM controllers using AVURPSO, GSA, and GA for transient stability improvement of a multi-machine power system with PV and wind farms," *Int. J. Electr. Power Energy Syst.*, vol. 106, pp. 455–466, Mar. 2019.
[23] M. I. Mosaad, "Model reference adaptive control of STATCOM for grid integration of wind energy systems," *IET Electr. Power Appl.*, vol. 12, no. 5, pp. 605–613, May 2018.
[24] M. J. Hossain, H. R. Pota, and R. A. Ramos, "Robust STATCOM control for the stabilisation of fixed-speed wind turbines during low voltages," *Renew. Energy*, vol. 36, no. 11, pp. 2897–2905, Nov. 2011.
[25] S. N. Sivanandam, S. Sumathi, and S. N. Deepa, *Introduction to Fuzzy Logic Using MATLAB*. Berlin, Germany: Springer-Verlag, 2007.
[26] L. Suganthi, S. Iniyan, and A. A. Samuel, "Applications of fuzzy logic in renewable energy systems—A review," *Renew. Sustain. Energy Rev.*, vol. 48, pp. 585–607, Aug. 2015.
[27] R. K. Sahu, S. Panda, and G. T. Chandra Sekhar, "A novel hybrid PSO-PS optimized fuzzy PI controller for AGC in multi area interconnected power systems," *Int. J. Electr. Power Energy Syst.*, vol. 64, pp. 880–893, Jan. 2015.
[28] B. K. Sahu, T. K. Pati, J. R. Nayak, S. Panda, and S. K. Kar, "A novel hybrid LUS–TLBO optimized fuzzy-PID controller for load frequency control of multi-source power system," *Int. J. Electr. Power Energy Syst.*, vol. 74, pp. 58–69, Jan. 2016.
[29] S. Behera, S. Sahoo, and B. B. Pati, "A review on optimization algorithms and application to wind energy integration to grid," *Renew. Sustain. Energy Rev.*, vol. 48, pp. 214–227, Aug. 2015.
[30] Y. del Valle, G. K. Venayagamoorthy, S. Mohagheghi, J.-C. Hernandez, and R. G. Harley, "Particle swarm optimization: Basic concepts, variants and applications in power systems," *IEEE Trans. Evol. Comput.*, vol. 12, no. 2, pp. 171–195, Apr. 2008.
[31] Y. Tang, P. Ju, H. He, C. Qin, and F. Wu, "Optimized control of DFIG-based wind generation using sensitivity analysis and particle swarm optimization," *IEEE Trans. Smart Grid*, vol. 4, no. 1, pp. 509–520, Mar. 2013.
[32] M. Alonso, H. Amaris, and C. Alvarez-Ortega, "Integration of renewable energy sources in smart grids by means of evolutionary optimization algorithms," *Expert Syst. Appl.*, vol. 39, no. 5, pp. 5513–5522, Apr. 2012.
[33] H. Huang and C. Y. Chung, "Coordinated damping control design for DFIG-based wind generation considering power output variation," *IEEE Trans. Power Syst.*, vol. 27, no. 4, pp. 1916–1925, Nov. 2012.
[34] C. Blum, "Ant colony optimization: Introduction and recent trends," *Phys. Life Rev.*, vol. 2, no. 4, pp. 353–373, Dec. 2005.
[35] A. Sakthivel, P. Vijayakumar, A. Senthilkumar, L. Lakshminarasimman, and S. Paramasivam, "Experimental investigations on ant colony optimized PI control algorithm for shunt active power filter to improve power quality," *Control Eng. Pract.*, vol. 42, pp. 153–169, Sep. 2015.
[36] Y. Eroğlu and S. U. Seçkiner, "Design of wind farm layout using ant colony algorithm," *Renew. Energy*, vol. 44, pp. 53–62, Aug. 2012.
[37] R. Rahmani, R. Yusof, M. Seyedmahmoudian, and S. Mekhilef, "Hybrid technique of ant colony and particle swarm optimization for short term wind energy forecasting," *J. Wind Eng. Ind. Aerodyn.*, vol. 123, pp. 163–170, Dec. 2013.
[38] M. S. Kıran, E. Özceylan, M. Gündüz, and T. Paksoy, "A novel hybrid approach based on particle swarm optimization and ant colony algorithm to forecast energy demand of Turkey," *Energy Convers. Manage.*, vol. 53, no. 1, pp. 75–83, Jan. 2012.
[39] F. Díaz-González, M. Hau, A. Sumper, and O. Gomis-Bellmunt, "Participation of wind power plants in system frequency control: Review of grid code requirements and control methods," *Renew. Sustain. Energy Rev.*, vol. 34, pp. 551–564, Jun. 2014.
[40] B. Singh and S. N. Singh, "Reactive capability limitations of doubly-fed induction generators," *Electr. Power Compon. Syst.*, vol. 37, no. 4, pp. 427–440, Mar. 2009.
[41] L. Meegahapola and S. Perera, "Capability constraints to mitigate voltage fluctuations from DFIG wind farms when delivering ancillary services to the network," *Int. J. Electr. Power Energy Syst.*, vol. 62, pp. 152–162, Nov. 2014.
[42] N. Senthil Kumar and J. Gokulakrishnan, "Impact of FACTS controllers on the stability of power systems connected with doubly fed induction generators," *Int. J. Electr. Power Energy Syst.*, vol. 33, no. 5, pp. 1172–1184, Jun. 2011.
[43] J. F. Conroy and R. Watson, "Low-voltage ride-through of a full converter wind turbine with permanent magnet generator," *IET Renew. Power Gener.*, vol. 1, no. 3, pp. 182–189, 2007.

OMAR MAKRAM KAMEL received the bachelor's and master's degrees in electrical engineering from the Faculty of Engineering, Minia University, Egypt, in 2008 and 2013, respectively, and the Ph.D. degree in electrical engineering (control of power systems), in 2018. Since January 2008, he has been working as an Assistant Lecturer with the Electrical and Computer Department, El-Minia Higher Institute of Engineering and Technology, Egypt. Since November 2018, he has been working with the Electrical and Computer Department, El-Minia H.I.E.T. His research interests are focused on power systems control, electric machine drives, and renewable energy systems.

AHMED A. ZAKI DIAB received the B.Eng. and M.Eng. degrees in electrical engineering from Minia University, Egypt, in 2006 and 2009, respectively, and the Ph.D. degree from Novosibirsk State Technical University, Novosibirsk, Russia, in 2015. He was a Postdoctoral Research Fellow with the Moscow Power Engineering Institute, Moscow, Russia for six months from 2017 to 2018. From July 2019 to December 2019, he was a Postdoctoral Researcher with the Green Power Electronics Circuits Laboratory, Kyushu University, Japan. He is currently working as an Assistant Professor with the Electrical Engineering Department, Faculty of Engineering, Minia University, Egypt. His current research interests include renewable energy systems, power electronics, and machines drives.

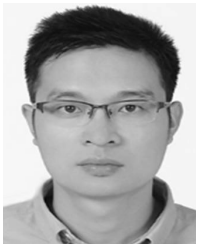

TON DUC DO (Senior Member, IEEE) received the B.S. and M.S. degrees in electrical engineering from the Hanoi University of Science and Technology, Hanoi, Vietnam, in 2007 and 2009, respectively, and the Ph.D. degree in electrical engineering from Dongguk University, Seoul, South Korea, in 2014.

From 2008 to 2009, he worked at the Division of Electrical Engineering, Thuy Loi University, Vietnam, as a Lecturer. He was with the Division of Electronics and Electrical Engineering, Dongguk University, as a Postdoctoral Researcher, in 2014. He was also a Senior Researcher with the Pioneer Research Center for Controlling Dementia by Converging Technology, Gyeongsang National University, South Korea, from May 2014 to August 2015. Since September 2015, he has been an Assistant Professor with the Department of Robotics and Mechatronics, Nazarbayev University, Kazakhstan. His research interests include the field of advanced control system theories, electric machine drives, renewable energy conversion systems, uninterruptible power supplies, electromagnetic actuator systems, targeted drug delivery systems, and nanorobots.

Dr. Do received the Best Research Award from Dongguk University, in 2014. He was also the Lead Guest Editor for the special issue of Mathematical Problems in Engineering on Advanced Control Methods for Systems With Fast-Varying Disturbances and Applications. He is currently an Associate Editor of IEEE Access.

MAHMOUD A. MOSSA received the bachelor's and master's degrees in electrical engineering from the Faculty of Engineering, Minia University, Egypt, in 2008 and 2013, respectively, and the Ph.D. degree in electrical engineering (control of electric machine drives), in April 2018. In January 2010, he was an Assistant Lecturer with the Electrical Engineering Department, Minia University. In November 2014, he joined the Electric Drives Laboratory (EDLAB), University of Padova, Italy, for his Ph.D. research activities. Since May 2018, he has been working as an Assistant Professor with the Electrical Engineering Department, Minia University. His research interests are focused on electric machine drives, renewable energy systems, power electronics, and smart grids.